Quark Propagation and Hadron Formation

A Proposal to PAC30

K. Hafidi[1], J. Arrington, L. El Fassi, D. F. Geesaman, R. J. Holt, B. Mustapha, D. H. Potterveld, P. E. Reimer, P. Solvignon

Argonne National Laboratory

K. Joo[1], M. Ungaro

University of Connecticut

G. Niculescu[1], I. Niculescu[1]

James Madison University

W. K. Brooks[1,2]

Jefferson Lab

M. Holtrop[1]

University of New Hampshire

K. Hicks[1], T. Mibe

Ohio University

L. B. Weinstein[1]

Old Dominion University

M. Wood[1]

University of Massachusetts, Amherst

G. Gilfoyle[1]

University of Richmond

H. Hakobyan[1]

Yerevan Physics Institute and Yerevan State University

and the CLAS COLLABORATION

[1]spokesperson
[2]contact person

Contents

List of Figures

List of Tables

1 Executive Summary

The confinement of quarks inside hadrons is perhaps the most remarkable feature of QCD. The quest to understand confinement quantitatively and in terms of intuitive physical pictures is an essential goal of modern nuclear physics. Much experimental attention has been focused on understanding confinement through hadron spectroscopy. Alternatively, the subject is often introduced through sketches of the hadronization processes by string-breaking. This picture is confirmed by lattice calculations using static quarks, showing that the gluon field is concentrated in a flux-tube (or string). In hadronization, the color string stretches until $q\bar{q}$ pairs tunnel up from the vacuum, thwarting the struck quark's attempt to escape to isolation. Unfortunately, the real picture with full QCD is more complicated than this simple picture, and lattice calculations of dynamical quarks are not yet possible. Experimental information is necessary to guide models of hadronization, to elucidate the mechanism of confinement. While sophisticated models for hadronization processes exist, they are only loosely constrained by data on particle production topologies.

The focus of the broad program of measurements and analyses proposed here has as its foundational goal to *determine the mechanisms of confinement in forming systems*. The essential experimental technique that enables these studies is to employ nuclei as analyzers of hadronization processes. In this approach, the hadron is formed from energetic quarks over distance scales ranging from 0–10 fm, i.e. the dimensions of atomic nuclei. The power of this technique arises from several factors: (1) the dimensions of the analyzing medium are perfectly matched to the distance scales of the hadronization process; (2) sophisticated knowledge about nuclear currents and properties can be exploited; (3) detailed experimental data on deep inelastic scattering from the nucleon provide a quantitative baseline against which to compare the data on nuclei. In essence, we use the nucleus as a "detector" to probe the hadronization formation length and the time scale on which a pre-hadron (such as a bare $q\bar{q}$ pair) becomes dressed with its own gluonic field. The response of the hadron to the presence of the nucleus depends on the time scale on which hadronization takes place inside the nucleus.

The hadronic multiplicity ratio R_M^h and transverse momentum broadening Δp_T^2 are the two primary observables developed herein. These are known to depend on at least four kinematic variables: ν, Q^2, z, and p_T^2, as well as the average distance through the nuclear medium, $\langle L \rangle$. These observables will be measured in deep inelastic kinematics for $x > 0.1$ in 60 days of 11 GeV beam on a series of 5–6 nuclei spanning the mass range 12–208. From these measurements, the quark production time will be determined and hadron formation

times will be extracted for a series of 15–20 hadrons. The production time τ_p is the lifetime of a deconfined quark, and it will be determined by analyzing the transverse momentum broadening Δp_T^2 as a function of $\langle L \rangle$ and ν; the length of the linear region essentially yields the production time. The formation times τ_f^h are the time intervals required to form the color field of hadrons, and these will be determined from the kinematic dependence of the hadronic multiplicity ratio R_M^h by using τ_p and models for interactions of pre-hadrons and hadrons in nuclei. Studying the systematic behavior of formation times for a variety of hadrons will determine the mechanisms by which hadrons are formed.

The measurements and analyses proposed here will provide two to three orders of magnitude more data than any previous measurement in this energy range, and will include a much larger collection of hadron species. The availability of 11 GeV beam in combination with the high rate capability of CLAS12 allows access to the ranges in ν, Q^2, and p_T^2 that are crucially needed to determine τ_p and to isolate the correct physical picture. These data will enable the multi-dimensional analysis that is crucial for discriminating between the competing models for these observables. The existing models are based on a variety of very different physical pictures. By providing a high-statistics, multi-dimensional analysis, the models with the correct physical picture can be validated, and significant new information on the mechanisms of QCD confinement in forming systems will be obtained.

2 Program Structure

This proposal is not for a single experiment, but rather for a *program* of measurements and analyses. The intention in presenting multiple experiments in a single proposal format is to convey the coherence of the program, which has at its core a few overarching goals. The optimal treatment of the data is to perform the analyses within a tightly coordinated framework, so that the results of the six experiments can be intercompared and interpreted as a whole.

Conditions common to all experiments: Deep inelastic scattering kinematics, study of hadronization processes, and 11 GeV beam on a series of five to six nuclear targets. In some cases there are limitations in particle identification, which is discussed in a later section in more detail, but all can be accessed over some range of momentum.

2.1 Experiment #1: Charged Pions and Protons

Spokespersons: Kawtar Hafidi (Argonne National Laboratory), Hayk Hakobyan (Yerevan State University), Kyungseon Joo (University of Connecticut), Lawrence Weinstein (Old Dominion University)

The study of the charged pions and the proton provides continuity to the HERMES studies; because the pions are high-rate, it is feasible to study the 'Cronin effect'[3] out to relatively high p_T and to study the multi-variable dependencies. These studies will have access to p_T broadening[4]

2.2 Experiment #2: Antiprotons

Spokesperson: Kawtar Hafidi (Argonne National Laboratory)

Because they are composed of antiquarks, antiprotons are very unlikely to contain the struck quark for $x > 0.1$. Thus, they provide an opportunity to identify and study exotic hadronization mechanisms for baryons. These studies will have access to p_T broadening.

---

[3]The Cronin effect is a modification of the transverse momentum spectrum of hadrons in p-A collisions compared to what is expected from a naive superposition of nucleon-nucleon collisions. Here it refers to the increase at high p_T of the hadronic multiplicity ratio, which may be closely connected

[4]defined in Eq. 12

2.3 Experiment #3: π^0, η, η'

Spokespersons: Gerard Gilfoyle (University of Richmond), Kyungseon Joo (University of Connecticut)

These channels, which require detection of two photons, explore the mass dependence of the formation lengths and help to probe any possible flavor dependence. No previous studies exist for the η and η'.

2.4 Experiment #4: $\omega, f1$

Spokesperson: Michael Wood (University of Massachusetts, Amherst)

These channels require a more complex analysis (three and four pions, including π^0) and probe the mass and flavor dependence to the maximum meson mass. No previous studies exist for these channels.

2.5 Experiment #5: Charged Kaons, K^0, ϕ

Spokespersons: Maurik Holtrop (University of New Hampshire), Ken Hicks (Ohio University)

Studying the formation of kaons offers several opportunities. The struck quark cannot be contained in a K^-, thus the hadronization mechanism must be exotic. For the K^0 and K^+ systems, for $z > 0.5$ there is a good probability that the struck quark is specifically identified as a d quark and u quark, respectively, thus the flavor of the struck quark is tagged. The ϕ probes the heavy meson sector in a system that has not been studied previously. These studies will have access to p_T broadening.

2.6 Experiment #6: Hyperons

Spokespersons: Gabriel Niculescu, Ioana Niculescu (James Madison University)

Study of hadronization mechanisms of the hyperons Λ, $\Lambda(1405)$, Σ^+, Σ^0, Ξ^0, Ξ^- will provide a wealth of completely new information on baryonic hadronization, an area in which even parametric models have not been particularly successful. The mass dependence can be studied over a mass range of 400 MeV. Flavor tagging may be feasible for some of these hadrons.

2.7 Analysis Coordination

The analyses of the six experiments will be coordinated by Will Brooks (Jefferson Lab).

3 Commitments of Collaborators to the 12 GeV Upgrade

3.1 Argonne National Laboratory

Argonne National Laboratory Medium Energy group is actively involved in this proposal, as well as in the color transparency proposal using CLAS12. Among CLAS12 baseline equipment, the group intends to take responsibility for the design, prototyping, construction and testing of the high threshold Cerenkov counter. 3 research staff and 2 engineers are likely to work at least part time on this project in the next few years. Funding for the group is from DOE. Additional sources of funding will be sought as appropriate. Beyond the baseline equipment, the group is also interested in exploring the possibility of building a RICH detector for CLAS12.

3.2 University of Connecticut

The University of Connecticut (UConn) group is actively involved in this proposal using CLAS12 baseline equipment.

Among the CLAS12 baseline equipment, our group is sharing the responsibility for the design, prototyping, construction and testing of the high threshold cerenkov counter (HTCC). One faculty member (Kyungseon Joo), one post-doc (Maurizio Ungaro), four graduate students (Bo Zhao, Nikolay Markov, Taisia Mineeva and Igor Konyukov) are already or will be working on this project.

The University of Connecticut Research Foundation (UCRF) already funded $32,000 for the equipment purchase for the HTCC prototyping project. UConn is also providing a clean room facility for this project and providing funding for a half postdoctoral support and a half graduate student support for the next two years for our group's JLab research activities. The group is currently funded by the U.S Department of Energy (DOE). Additional sources of funding will be sought as appropriate.

Beyond the baseline equipment, the group is also deeply involved in software planning and development for CLAS12. The group was recently awarded a DOE SBIR/STTR Phase I grant with a software company, CyberConnect EZ to develop a software framework to archive a large scale nuclear physics experiment data base.

3.3 James Madison University

James Madison University is actively involved in this proposal using CLAS12. Among CLAS12 baseline equipment, the group intends to make important contribution to the prototyping, construction and testing of the pre-shower calorimeter. Three faculty members are likely to work at least part time on this project in the next few years. Funding for the group is from NSF and we have a strong undergraduate research component. Additional sources of funding will be sought as appropriate.

3.4 Jefferson Lab

The Jefferson Lab group is actively involved in this proposal, as well as in one LOI using CLAS12, and no other proposals for Hall A, C or D. For the CLAS12 baseline equipment, the group is involved full-time in project management for CLAS12 as well as for the 12 GeV Project Experimental Equipment for Halls A, C, and D. Beyond the baseline equipment, the group is also interested in exploring a RICH detector in at least one sector for CLAS12, should funding become available.

3.5 University of Massachusetts

The University of Massachusetts at Amherst is actively involved in this proposal using CLAS12. Michael Wood, a postdoctoral researcher with the group, has experience with vector meson production off heavy nuclear targets from the E01-112 experiment. He is a spokesperson on a PAC30 proposal "Search for Modification of Vector Meson Properties in Nuclei". Currently, his planned contribtributions to CLAS12 are with software and simulation development.

3.6 University of New Hampshire

The University of New Hampshire Nuclear Physics group is actively involved in this proposal, as well as in 3 other proposal using CLAS12. The UNH group is committed to significant contributions in the development of the CLAS12 software. Maurik Holtrop is currently chair of the CLAS12 GEANT4 simulation group to which our post-doc Hovanes Egiyan is also contributing. Since currently the main software efforts for CLAS12 are in the area of simulation we are also part of and contributing to the general CLAS12 Software group. Current manpower commitments to this effort are 0.15 FTE of a faculty and 0.4 FTE of one post-doc. We expect to increase this effort as our CLAS activities wind down and our

CLAS12 activities pick up and we expect to attract some talented undergraduate students to this project. Among CLAS12 baseline equipment, the group intends to take responsibility for the design, prototyping, construction and testing of the silicon vertex detector and perhaps the inner detector's silicon tracking detectors. Faculty member Maurik Holtrop is likely to work at least part time on this project in the next few years and is likely to be joined by Jim Connel, a cosmic ray experimentalist with a background in nuclear physics, who is very interested in joining the vertex detector project. He has considerable experience with silicon detectors for space observations. Funding for the group is from DOE and additional sources of funding will be sought for this project to bring Prof. Connel aboard. If funded, we are likely to devote a post-doc, a graduate student and one or two undergraduate students to this project. Beyond the baseline equipment, the group is also interested in exploring an extended inner calorimeter for CLAS12.

3.7   Ohio University

Ohio University is actively involved in this proposal using CLAS12, with emphasis on the analysis of kaon and phi hadronization. Of the CLAS12 basline equipment, the group will make important contributions to the prototyping, construction and testing of the pre-shower calorimeter, in conjunction with Jefferson Lab staff led by Stepan Stepanyan. The group currently consists of one faculty member, one postdoc and one graduate student, and future contributions to the CLAS12 detector development will depend on continued funding from the NSF. Additional funding from Ohio University and other sources will be sought as appropriate. Provided that the group remains funded, they are committed to the pre-shower calorimeter project, and will contribute by allocating full-time on-site participation by the graduate student, with guidance by Stepanyan, along with half-time on-site participation by the post-doc and part-time participation by the faculty member (who is located off-site). Both post-doc and faculty member are experienced in hardware development and in addition will provide analysis expertise to document the results of the prototype tests and comparison with simulations using the GEANT4 software package. Beyond the baseline equipment, the group is interested in investigating the possibility of placing neutron detectors at backward angles for measurement of the nuclear response to DIS hadronization, as an extension of measurements done at Fermilab (E665 experiment) by the Ohio University group and published in Physical Review Letters.

3.8 Old Dominion University

The Old Dominion University group is actively involved in this proposal, as well as several other proposals using CLAS12. Other members of our group are pursuing a proposal for Hall A, but their contributions are not included here. Among CLAS12 baseline equipment, the group intends to take responsibility for the design, prototyping, construction and testing of the Region 1 Drift Chamber. Five faculty (including one research faculty) and one technician are likely to work at least part time on this project in the next few years. Funding for the group is from DOE and from the university (75% of research faculty salary + one regular faculty summer salary + 50% of the technician). The university has also provided 6000 square feet of high bay laboratory space with clean room capabilities for our use. We will seek other sources of funding as appropriate. Gail Dodge is the chair of the CLAS12 Steering Committee and the user coordinator for the CLAS12 tracking technical working group. Beyond the baseline equipment, the group is also interested in exploring improvements to the BoNuS detector and a future RICH detector for CLAS12.

3.9 University of Richmond

The University of Richmond group is actively involved in this proposal using CLAS12. Among CLAS12 baseline equipment, the group intends to take responsibility for the design, prototyping, development and testing of software for event simulation and reconstruction. One faculty member along with 2-3 undergraduates each year are likely to work at least part time on this project in the next few years. The group has a 100-CPU computing cluster solely for nuclear physics supported by a linux-trained, technical staff member. The cluster was funded by NSF and the University. The University also supports routine travel to Jefferson Lab and undergraduate summer stipends. Funding for the group is from DOE. Additional sources of funding will be sought as appropriate.

4 Physics Discussion

4.1 Confinement Mechanisms and Experimental Observables

An elementary view of confinement mechanisms in deep inelastic scattering is afforded by the string model or "color flux tube model" [9][13]. This is one of the foundations upon which the Lund hadronization model is constructed. In this picture, a quark removed from a hadron forms a string or 'chromo-electric flux tube' which extends over a space-time region. The string has a 'tension' κ with a magnitude of approximately 1 GeV/fm in free space. Given adequate energy, $q\bar{q}$ pairs can tunnel up from the vacuum and 'break' the string into two strings. The probability of quark pair production per unit time and per unit length is given by the Schwinger formula [32][13]

$$W = \frac{\kappa}{2\pi^3}\exp(-\frac{\pi m_q^2}{2\kappa}), \tag{1}$$

(or its modern equivalent, in which $m_q^2 \to m_q^2 + p_T^2$). Equation 1 shows that the probability of quark pair production depends on the ratio of quark mass squared to the string tension parameter. Because the light quark masses are significantly less than 1 GeV, the string length is, in this picture, typically less than 1 fm.

While the string model has been a useful basis for phenomenological analyses of hadronization phenomena, it is far too crude to provide a microscopic picture of the confinement of quarks in forming systems. The fundamental degrees of freedom in QCD, quarks and gluons, must be invoked in any detailed description. Cluster models such as the one employed in HERWIG [14] are a first step in the right direction, but are still highly phenomenological in nature.

One class of confinement observable that can be isolated is the *characteristic times* for distinct stages of the hadron formation process. The initial stage is the absorption of a virtual photon by a quark on a time scale that is presumably brief, $\ll$ 1 fm/c, and which is governed by the virtual photon wavelength. There must follow a stage during which the colored quark propagates over a distance as essentially a quasi-free particle, and in this stage the quark radiates gluons with a differential spectrum given by pQCD as

$$dw^{q\to qg} = \frac{\alpha_s(k_\perp^2)}{4\pi}2\frac{4}{3}[1 + (1 - \frac{k}{E})^2]\frac{dk}{k}\frac{dk_\perp^2}{k_\perp^2} \tag{2}$$

where E is the quark energy, k_μ is the 4-momentum of the gluon and $k_\perp$ is the gluon transverse momentum. The characteristic time associated with this stage has been called the *production time* by various authors [26]:

production time: the time interval during which a quark is deconfined

The production time is a characteristic of a propagating quark, and in principle it should be independent of which final state hadron is formed.

In a third stage of the process, the gluon radiation ceases, which can only happen if the struck quark has found partner quarks to neutralize its color. During this stage, a 'pre-hadron' evolves to become an 'ordinary' hadron. This characteristic time is the _formation time_ for the hadron:

formation time: the time required to form the color field of a hadron

Unlike the production time, the magnitude of the hadron formation time is expected to depend in detail on the hadron species being formed.

The existence of the production time and the formation time is dictated by two of the most fundamental properties of QCD, namely, that a colored quark can only propagate for a limited distance (confinement), and the equilibrium color field of a hadron cannot be formed instantaneously (causality).

Production Time

It is possible to obtain simple estimates for the production time from basic considerations. To a very good approximation, in deep inelastic kinematics and at $x > 0.1$ [1], the struck quark absorbs all the energy of the virtual photon. Thus, the initial energy of the struck quark is known to be ν, neglecting the quark's mass. Conservation of energy dictates that the final energy of the hadron containing the struck quark must be no greater than ν. If, however, the quark radiates gluons as it propagates, this constitutes a loss in energy which drives the hadron's energy below ν. The energy loss due to gluon emission can be estimated from the string model: the main parameter of the string model is the string tension κ, where $\kappa \approx 1$ GeV/fm. In the string model there is no explicit gluon emission, however, the growth of the string creates an effective energy loss for the struck quark that is governed by the value of κ. Thus, in this picture, the best estimate for the rate of (vacuum) energy loss is:

$$\frac{dE}{dx}\Big|_{vacuum} \approx 1 \ \ \text{GeV/fm.} \tag{3}$$

---

[1] below $x \approx 0.1$, a different mechanism begins to contribute, see the section entitled :Space-Time Picture of Nuclear Deep Inelastic Scattering."

If $z_h = E_h/\nu$ is the fraction of the struck quark's initial energy retained by the hadron, then $\nu(1 - z_h)$ is the energy lost through gluon emission by the struck quark. Thus an estimate of the distance over which gluons are emitted is

$$l_p = \frac{\nu(1 - z_h)}{\kappa}, \tag{4}$$

the production length (production *time* is $\tau_p = l_p/c$). This result was first noted in the 1980's [27][28].

For example, for a 5 GeV pion with $z_h = 0.6$, $l_p = 3.3$ fm. Thus, the production time is expected to be of the order of a few fm at JLab energies.

A more sophisticated estimate of the production time can be obtained from pQCD using the coherence time, which is the time required to radiate a photon or gluon:

$$l_c = \frac{2Ex(1 - x)}{k_T^2 + x^2 m_q^2}. \tag{5}$$

In this expression, x is the fraction of the quark energy carried by the gluon, m_q is the quark mass, E is the quark energy, and k_T is the intrinsic transverse quark momentum squared. Using $\frac{dn_g}{dz} \approx 1/z$ [30][19] and integrating over a path L yields the expression for the rate of vacuum energy loss

$$\frac{dE}{dx}|_{vacuum} = -\frac{2\alpha_s}{3\pi}Q^2. \tag{6}$$

For $Q^2 = 1$ GeV^2, taking $\alpha_s = 0.4$ gives $\frac{dE}{dx} = 0.4$ GeV/fm, somewhat smaller than the value of κ from the string model, implying the production length is 2.5 times longer than mentioned above. Now, however, in distinction to the string model, there is a strong Q^2 dependence. Thus for the pion in the example above, using the perturbative expression, $l_p = 8$ fm for $Q^2 = 1$ GeV^2, but it would shrink to $l_p = 1$ fm at 9 GeV^2 (the upper limit accessible in the proposed experiment with 11 GeV beam). Thus pQCD predicts that the production time will decrease with increasing Q^2, an effect that can be tested experimentally with the proposed measurements.

Hadron Formation Time

The second example of a characteristic time is the *hadron formation time*. Unlike the production time, the formation time is not directly related to the confinement property of QCD; rather, it is a measure of the time required to form the non-perturbative color field of the hadron starting from a small color-singlet object. This field-regeneration time has a well-known analog in QED.

16

It is possible to construct simple estimates for the formation time. To form a hadron of radius R starting from a pointlike, bare color singlet object, the speed at which the field can arise in its rest frame is bounded by the speed of light:

$$\tau_{formation}^{rest} > \frac{R}{c}. \tag{7}$$

In the lab frame, the Lorentz boost adds an additional factor for time dilation:

$$\tau_{formation}^{lab} > \frac{E}{m^*} \frac{R}{c} \tag{8}$$

where m^* is the mass of the propagating color-singlet object. In principle, m^* ranges from the mass of two bare quarks at a minimum to the fully formed hadron mass m_h at a maximum. A lower limit for the formation time is given by setting $m^* = m_h$.

While the above estimate has been posed as a classical calculation, a quantum mechanical analysis that takes into account the gluon wavelengths involved arrives at the same formula [15]. The Fourier component of the gluonic field associated with the longest wavelengths $\lambda \approx R$ takes the longest time to come to full strength, and this sets the scale of the hadron formation time. In this quantum-mechanical picture, the assumption of a pointlike initial configuration made in the paragraph above is no longer necessary, since the lowest-momentum wavefunction components control the completion of the hadron formation process.

To give a concrete example using formula 8 above, for a 5 GeV pion with a radius of 0.7 fm, the formation time estimate is

$$\tau_{formation}^{lab,\pi} > 25 \ \ \text{fm} \tag{9}$$

This simplistic estimate sets the scale for formation times: pion formation times are expected to be of order 10 fm at JLab energies.

4.2   Space-Time Picture of Nuclear Deep Inelastic Scattering

The section above addressed the quark production time and hadronic formation time. These quantities can be deduced by using the nuclear medium as an analyzer. The space-time picture of nuclear deep inelastic scattering, and how it can be used to measure these characteristic times, is the subject of this section, which follows the development by Brodsky et al. [16].

In deep-inelastic leptoproduction of hadrons, the presence of the nuclear medium in the final state may modify the hadronization process. The postulate that the process of hadron
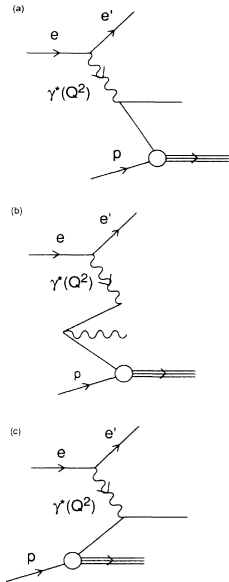
Figure 1: Time-ordered contributions to DIS in the target rest frame. Taken from [16].
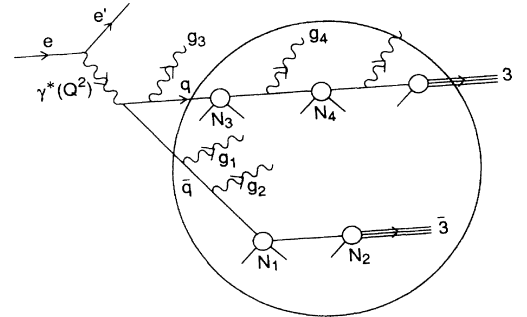

Figure 2: DIS in a nuclear target in the target rest frame. Taken from [16].

creation has an intrinsic formation time implies that at higher energies the entities interacting with the medium are quarks and and gluons. These interactions with the nucleus can resolve the space-time structure of fundamental QCD processes at fermi-size scales. In order to take advantage of the wealth of knowledge about nuclear properties it is advantageous to analyse the interactions in the target rest frame. The dominant time-ordered processes in the laboratory frame are shown in Fig. 1. The uppermost diagram of quark-pair creation dominates for $x < 0.1$, while the lowest diagram, where the virtual photon is absorbed by a single valence quark, dominates for $x > 0.1$. For simplicity of interpretation of the data, all analyses in this proposal are constrained to $x > 0.1$. In this case, ν is simply the initial energy of the quark, and $z = E_h/\nu$ is to a good approximation the fraction of the struck quark's energy carried by the final hadron for $z >\approx 0.5$.

Fig. 2 shows the general case of a high-energy interaction in the presence of a nucleus. In this case a quark pair is created and both quark and antiquark travel through the nuclear medium. The propagating quarks emit gluons, both outside and inside the medium. As they propagate through the medium, they multiple scatter, which broadens their transverse momentum. In the final stage, the quarks hadronize into a jet of hadrons, which may occur inside or outside the nucleus.

To specialize to the picture of primary interest in this proposal, Fig. 3 shows the scenario where the struck quark fully absorbs the virtual photon (no quark pair production occurs) and in that case the transverse momentum broadening can be measured directly from the direction of the virtual photon. In this picture, the hadronization process is not shown; the quark exits the nucleus and hadronization completes at a later stage.

If hadronization occurs within the nucleus, additional effects can be observed. It is expected that once the quark has stopped radiating gluons it will evolve to a color singlet object (by picking up an antiquark or two other quarks, forming a meson or baryon). This color singlet object now can in principle interact with the medium without needing to transfer color charge; it is referred to as a 'pre-hadron.' Following its formation, the pre-hadron evolves to a full hadron, in which form it can clearly interact with the nuclear medium. Thus, in the case where a pre-hadron or hadron form within the nucleus, there is the possibility of a 'violent' interaction with the medium, which removes particle flux relative to the same conditions on a smaller nucleus such as deuterium. This is referred to as 'hadron attenuation' and it is observed experimentally through the use of the 'hadronic multiplicity ratio':

$$
R_M^h(z, \nu, Q^2, p_T) = \frac{\left\{ \frac{N_h(z, \nu, Q^2, p_T)}{N_e^{DIS}(\nu)} \right\}_A}{\left\{ \frac{N_h(z, \nu, Q^2, p_T)}{N_e^{DIS}(\nu)} \right\}_D}
\tag{10}
$$

In this expression, N_h is the number of hadrons produced in DIS events and N_e^{DIS} is the number of associated DIS electrons. The numerator corresponds to target nucleus A, and the denominator corresponds to deuterium. ν is the energy transferred by the electron, and z is the hadron energy divided by ν ($0 < z < 1$). In the QCD-improved parton model, R_M^h is given by ratios of sums over products of the quark distribution functions with fragmentation functions.

4.3   Theoretical Approaches

Much theoretical work was stimulated by the European Muon Collaboration's data in the early 1980's [10] comparing F_2 in heavy nuclei to light nuclei, and ultimately uncovering the famous 'EMC' effect. An example of such theoretical work is the effort by Jaffe, Close, Roberts, and Ross [23] which proposed that the nuclear medium slightly modified the confinement scale for bound nucleons and suggested a non-zero probability for multi-quark configurations in nuclei beyond the ordinary baryons. A collection of models accumulated
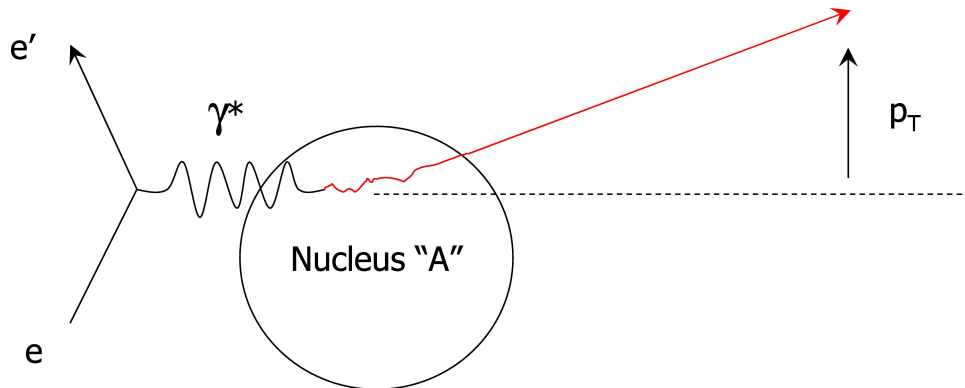
Figure 3: Schematic cartoon of transverse momentum broadening for the dominant DIS process for $x > 0.1$.

as a consequence of these data, many not able to be tested against data until the advent of the HERMES nitrogen measurements [7] for hadron attenuation beginning in the late 1990's. The HERMES data immediately ruled out several of these model predictions for how hadron attenuation would behave at high z Since that time HERMES has published more data for krypton targets, including fully identified hadrons in the final state. These beautiful data have stimulated a new wave of modeling from various points of view. All of the new models are able to describe the HERMES data in some measure, although they are based on somewhat different physical pictures. A very brief account will be given here; the reader is referred to one recent paper for each approach if more background information is desired. Before describing the hadron attenuation models, a brief mention on Lattice QCD and the pQCD calculations of quark energy loss by BDMPS will be given.

4.3.1 Lattice

Ideally one would confront hadron attenuation data with Lattice QCD. Initially this would seem nearly impossible for technical reasons: a Minkowski space calculation is needed, and a non-zero baryon density medium is needed. These are technical challenges with at least a 5–10 year time horizon. However, there may be some alternative approaches. These measurements are intended to determine what happens in vacuum hadronization by examining the small modifications brought about by the nuclear medium, and interpreting the data in terms of what is known about nuclei. Thus, the simpler questions really being asked are: how long does it take for two bare quarks to expand to a full-sized pion, and how does it

happen? how far can a quark of a given energy propagate before its color is neutralized? While still far from mainstream lattice topics, there are a few calculations that begin in a primitive way to address these simpler questions. Still, it will be many years before there could be hoped to be any firm conclusions from the lattice on these topics.

4.3.2 BDMPS and Quark Energy Loss

There has been a long series of calculations in perturbative QCD by Baier, Dokshitzer, Mueller, Peigne, and Schiff addressing the topic of quark energy loss in both cold and hot nuclear matter. For a review, see [11]. Using perturbative QCD, they connect the transverse momentum broadening[5] to medium-stimulated quark energy loss via a simple formula:

$$\frac{dE}{dx}|_{medium} = \frac{3}{4}\alpha_s \Delta p_T^2. \tag{11}$$

The mechanism of energy loss is primarily medium-stimulated gluon radiation, although collisional losses are also treated. Although they do consider 'cold' nuclear matter (i.e., nuclei), they do not specifically address the HERMES data.

4.3.3 Gluon Bremsstrahlung Model

The gluon bremsstrahlung model [26] pre-dates the HERMES data by several years, and thus it constitutes an actual prediction that fits the data well. In its initial form it addressed leading pions ($z > 0.5$) but has now been expanded to include positive kaons. It emphasizes the role of hadronization in explaining the HERMES data; medium-stimulated energy loss has only a small effect in this approach. The proponents extend the consequences of their conclusions to relativistic heavy ion collisions.

4.3.4 Twist-4 pQCD Model

The twist-4 pQCD model[35] builds on more than a decade of development focusing on how radiative energy loss of quarks by gluon emission can be used to identify and study the quark-gluon plasma. In this approach, the leading twist-4 term in the twist expansion is weighted with a coefficient; the coefficient may be determined for one nucleus, and then can be used to predict hadron attenuation for another nucleus. The conclusions can also be extended to hot nuclear matter. In this approach, hadronization plays no role whatsoever in the HERMES data; it is explained entirely by medium-stimulated gluon emission.

---

[5]An increase in the average transverse momentum relative to the initial direction of the quark due to interactions in the medium; discussed in detail in the following section

4.3.5 BUU Model

The BUU model approach[18] has also been developed over a long period of time, and has been tested against many kinds of data with considerable success. It treats final states with high accuracy via a coupled-channel approach using classical transport equations. As applied to the HERMES data, it uses a PYTHIA 'front end' to generate the initial state and the machinery of the BUU code to predict the outcome. An important result from this work is that in order to successfully reproduce the HERMES data, it is necessary to introduce a simple hadron formation length; without this step, the data clearly would disagree with this very mature calculation. They argue that some form of 'prehadron' needs to be invoked in any description of the data.

4.3.6 Arleo Model

The Arleo Model [8] is a much more fully developed description of the HERMES data using the interpretation that hadronization plays a minor role and that radiated gluons play the larger role. The model agrees with the data broadly, and the nature of the disagreements where they occur (e.g. at high z) suggest that hadronization as an effect is still present, but is a relatively small effect.

4.3.7 Rescaling Models and Two-Time-Scale Models

The rescaling models [1] revive the ideas from the 1980s that the confinement scale for the bound nucleon may be somewhat different from vacuum, and while it is a small effect, they demonstrate that it is enough to potentially reproduce most of the features of the HERMES data. This group has subsequently turned to modeling that includes multiple characteristic times corresponding to distinct subprocesses: formation of a string, and formation and attenuation of a prehadron. They are able to describe the HERMES data in this approach, which emphasizes hadron 'absorption,' i.e., hadronic interaction with the nuclear medium.

4.4 Extraction of Characteristic Times from Data

The strategy for extracting characteristic times from the data makes use of the interactions of the propagating quark and subsequent hadrons with the nuclear medium. This approach permits direct observation of physics at the femtometer scale, which is the natural scale for studies of quark propagation and hadron formation.

The relevant interactions with the nucleus fall into two classes: the gentle perturbations on the trajectory of the de-confined quark caused by partonic-level multiple scattering, and the violent interaction of ordinary hadrons and pre-hadrons that transfers flux from one channel to another. The first interaction, medium-induced partonic multiple scattering, yields sensitivity to the production time τ_p, since it only occurs when the colored quark is propagating and emitting gluons. Experimentally it is determined by *transverse momentum broadening*. The second interaction, hadronic interaction with the nucleus, signals the time of formation of the hadron, τ_f. Experimentally it is observed by *hadron attenuation*.
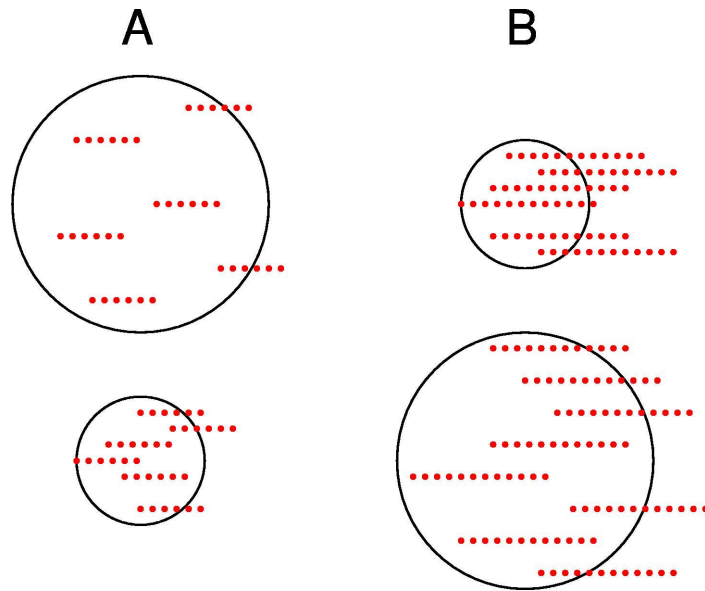

Figure 4: A schematic cartoon indicating the physical picture of the production time. The production time is represented by a dotted line and a larger and smaller nucleus are indicated by the two circles. The production time in the two nuclei under the label 'A' is less than the diameter of either nucleus, and thus an increase in the production time will produce a corresponding increase in the average dE/dx or Δp_T^2 measured. For the two nuclei in column 'B' the production time is equal to the diameter of the smaller nucleus, thus an increase in the production time will only result in the average dE/dx or Δp_T^2 increasing for the larger nucleus; the smaller nucleus is saturated.

4.4.1 Extracting the production time

The production time can be measured through observing the length dependence of transverse momentum broadening, or p_T broadening (which is in pQCD directly associated with
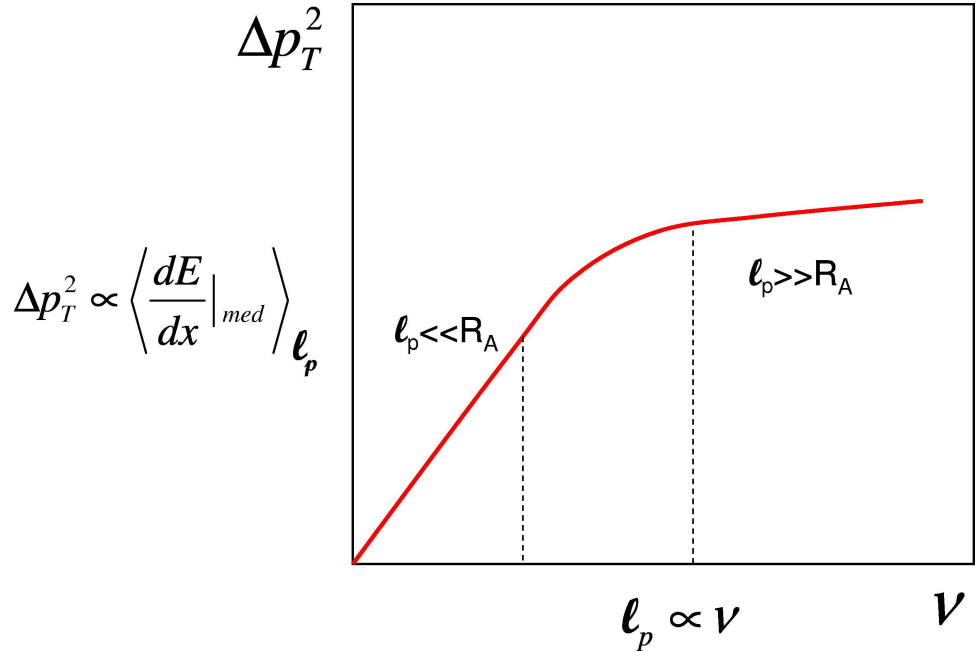
Figure 5: A schematic plot of the expected dependence of Δp_T^2 vs. ν. As emphasized by the equations next to each axis, this is equivalent to a plot of the medium-induced dE/dx, averaged over l_p, vs. l_p. For values of l_p that are much smaller than the nuclear radius R_A, the averaged dE/dx is proportional to l_p. Once the production rate grows to be much larger than l_p, the averaged dE/dx plateaus.

partonic energy loss, dE/dx, through medium-stimulated gluon emission, see Eq. 11 and Eq. 12). The broadening occurs only during the phase wherein the colored quark emits gluons that are stimulated by the medium. By determining the length dependence of the broadening as a function of all the relevant variables (Q^2, ν, z, p_T,and nuclear radius R_A) it is possible to infer the time scale τ_p over which the quark is de-confined. A primitive analysis can be performed essentially on inspection of the data, however, a sophisticated analysis is required for a quantitative understanding. The framework for the fully sophisticated analysis will be developed over the next few years in conjunction with the international community of theorists engaged in these topics.[6]

The principles of the method are illustrated in Fig. 4. The circles represent nuclei of two different diameters, and the dashed lines represent the distance traveled by the propagating

---

[6]For a recent workshop on these topics representing a portion of this community, see http://conferences.jlab.org/ECT/program.html

colored quark. The left edge of the dashed line must fall within a circle since the struck quark originates from within the nucleus, while the right edge of the dashed line can extend out of the nucleus. The propagation of pre-hadrons or hadrons is not shown, only the production length $l_p = c\tau_p$ is represented.

The nuclei in column "A" in Fig. 4 are larger in diameter than the production length l_p, which is shown as a constant length. Thus any elongation of the production length will be reflected in increased p_T broadening and medium-induced energy loss dE/dx.

The nuclei in column "B" in Fig. 4 are shown with a longer production length l_p. The production length is equal to the diameter of the smaller nucleus. Any elongation of the production length will not produce greater p_T broadening in the smaller nucleus, while it will do so in the larger nucleus; the smaller nucleus is saturated. A plot of p_T broadening vs. production length would show a plateau for the smaller nucleus for production lengths longer than what is shown in column "B", while it would continue to rise for the larger nucleus. (In a real nucleus, the edge is diffuse, thus the plateau would not be expected to be perfectly horizontal but could have some small slope.)

This effect is further illustrated in Fig. 5, which is a plot of p_T broadening vs. ν for an unspecified larger nucleus A of radius R_A. Here p_T broadening for nucleus A relative to deuterium is defined by:

$$\Delta p_T^2 = p_T^2(A) - p_T^2(^2H) \tag{12}$$

and it is taken as proportional to the partonic energy loss dE/dx as indicated on the figure. Since the production time τ_p is elongated by time dilation, then the lab frame production length l_p is proportional to the hadron energy $E_h = \nu z$, i.e. it is proportional to ν for fixed z. Fig. 5 shows a region of proportionality for lower ν followed by a plateau region at higher ν. This is the natural consequence of the length of the multiple scattering process saturating the nucleus.

To further illustrate this effect, Fig. 6 shows preliminary π^+ data from the CLAS EG2 experiment at 5.0 GeV. These data are for Q^2 from 1 to 2 GeV^2, and for z from 0.5 to 0.6, corresponding to the expected region of longest production length, and where there is a good probability that the measured hadron contains the struck quark. The three curves are for carbon (bottom), iron (middle), and lead (top) targets. These data suggest the plateauing behavior discussed above. The ordering (larger nucleus on top, smaller nucleus on bottom) is also completely consistent with the picture discussed. It is clear that extending these data to much higher ν with 11 GeV beam will be very important for testing the validity of this picture and for quantitative extraction of the production length. With 11 GeV beam a number of important tests can be carried out, such as doubling the range of ν to see if

a plateau is actually formed and to test if models reproduce it, to test the Q^2 dependence referred to in the perturbative calculation of 6, and to have sufficient phase space to study the effect of traditional treatments of hadronization, such as varying rapidity cuts, which may allow a broader region of z to be explored.
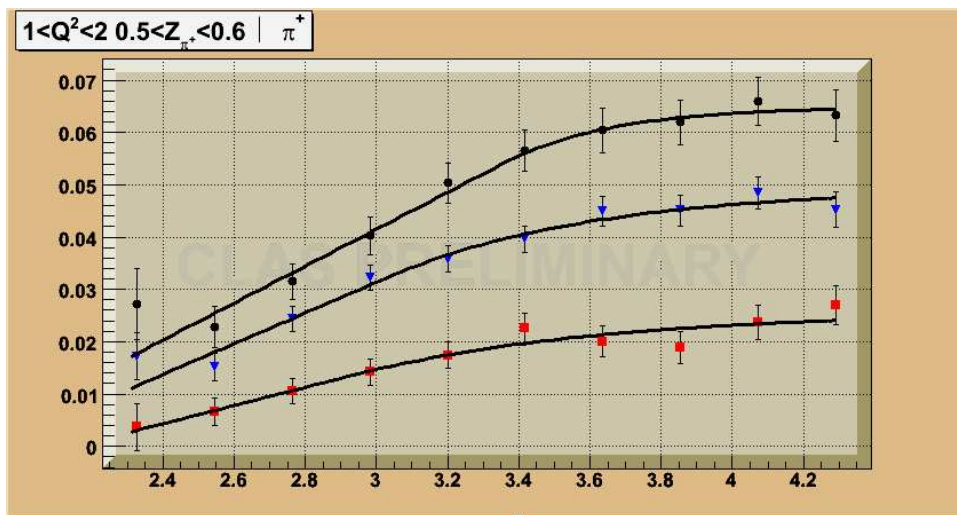

Figure 6: Preliminary data from the CLAS EG2 run for Δp_T^2 (GeV^2) vs. ν (GeV) for carbon(bottom), iron (middle), and lead(top) for a bin in Q^2 and z. The lines are fits using a simple function to guide the eye. The data suggest the plateauing behavior referred to in Fig. 5, consistent with saturation of the production length l_p.

The essential information on the production length from Fig. 6 consists of two features: the region of transition to the plateau, and the spacing between the three curves. This spacing can be plotted independently, and it may in fact be more sensitive to the production length. To illustrate this point, Fig. 7 shows a plot of Δp_T^2 vs. $A^{1/3}$, which is proportional to the nuclear radius. For very large production lengths, the curve should be a straight line: the thicker the nucleus, the greater the extent of multiple scattering, partonic energy loss, and the consequent p_T broadening. For shorter production lengths, the curve is expected to fall below the straight line starting at the point where the production length begins to be comparable to the nuclear radius. This is a very direct signal of the finite extent of the production length.

To illustrate this point, Fig. 8 shows preliminary π^+ data from the CLAS EG2 experiment at 5.0 GeV. These data are for z from 0.6 to 0.7 and for two bins in (Q^2, ν) of (1–2, 2–3) and (2–3 GeV^2, 3–4 GeV). The $(1-z)$ term in Eqn. 4, which arises from energy conservation,
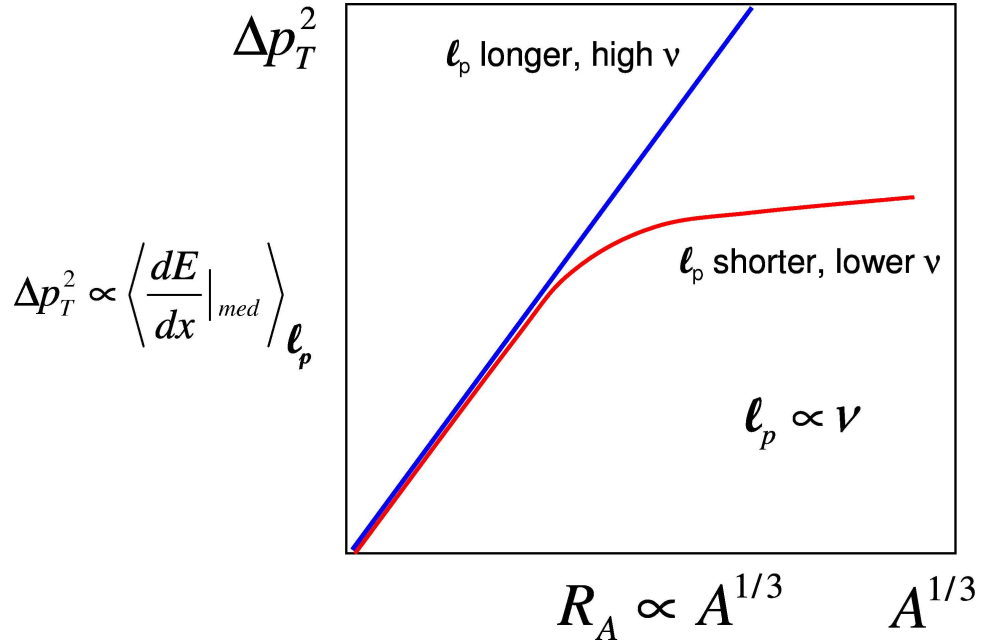
Figure 7: A schematic plot of the expected dependence of Δp_T^2 vs. $A^{1/3}$. As emphasized by the equations by each axis, this is equivalent to a plot of the medium-induced dE/dx, averaged over l_p, vs. the nuclear radius R_A. For larger values of ν, corresponding to larger values of l_p, the averaged dE/dx grows proportionally with the nuclear size. For smaller values of ν, corresponding to smaller values of l_p, the averaged dE/dx drops below the line at larger values of $A^{1/3}$ since the nuclear diameter becomes larger than l_p.

suggests that l_p should be somewhat shorter than it is in the previous plots for $z = 0.5$. While for lower z the plots in general show a linear behavior within the uncertainties, Fig. 8 suggests a tendency of the data to saturate rather than follow a straight line. With only three data points (corresponding to three target nuclei) it is difficult to precisely extract the point at which there is a departure from a linear behavior; further study is needed to determine the uncertainties which will ultimately be achievable. By visual inspection of this plot, if a plateauing behavior were assumed to be correct, it would appear that the production length for these kinematics is in the range of 3–4 fm. At 11 GeV it is desirable to have at least five or six targets in order to map this out more reliably and precisely. However, the basic behavior is very suggestive and is consistent with the schematic drawing in Fig. 7 and the ideas it represents.

The production time is expected to be a property of the de-confined quark and should in principle not depend on which final state hadron is formed. Thus, the analysis of varying
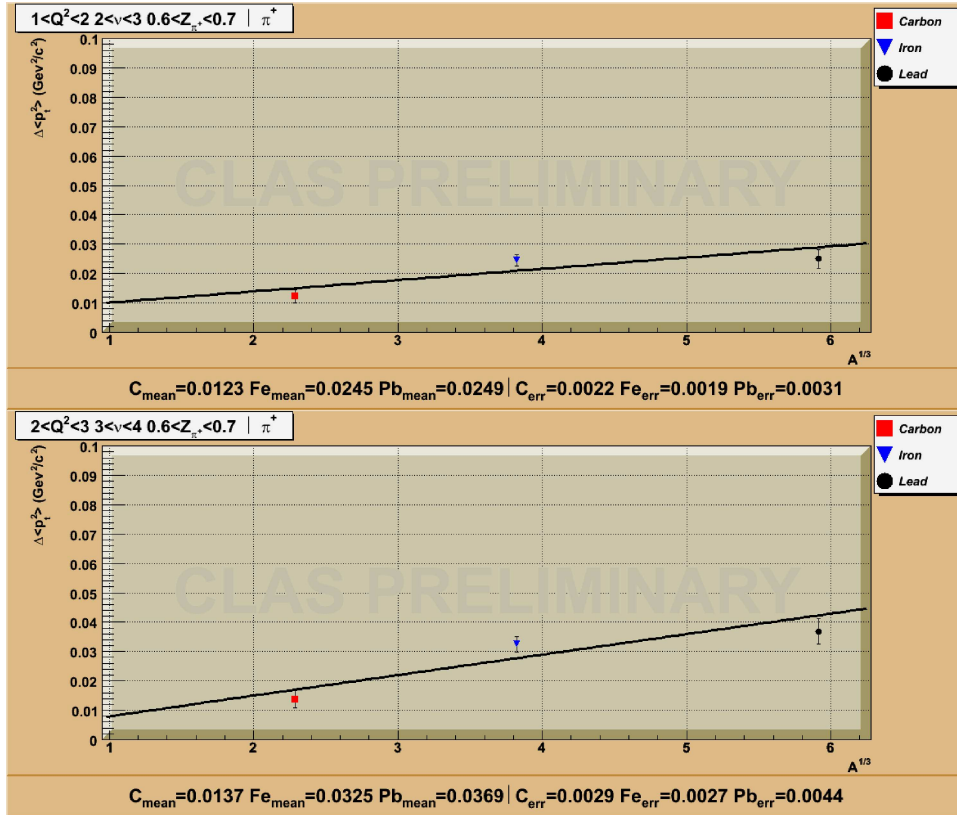
Figure 8: Preliminary data from the CLAS EG2 run for Δp_T^2 vs. $A^{1/3}$ for carbon, iron, and lead for two bins in Q^2, ν, and z. The lines are linear fits to guide the eye. The data suggest the plateauing behavior referred to in Fig. 7, consistent with saturation of the production length l_p.

hadron species should yield a consistent value for the production time. In the program proposed here, Δp_T^2 is accessible for hadrons detected via final states which only include charged particles. This is because the high precision of the CLAS12 silicon vertex tracker and the drift chambers is adequate to yield good p_T^2 resolution, but the moderate angular and energy resolution of the forward calorimeter is not. The most straightforward measurement should be from the charged pions, and perhaps the charged and neutral kaons. Cross-checks of varying relevance may be possible using the ϕ, proton and anti-proton, Λ and Ξ^-, however, any possible relevance of these to the extraction of the production length requires further study.

There are a few corrections to be applied to Δp_T^2. In principle, Fermi motion could contribute to the broadening. This correction, however, is suppressed by a factor of $x^2 z_h^2$[25]

and thus is smaller than the expected experimental resolution. A second effect that can be considered is any contribution from a pre-hadron or hadron to the broadening. At high z, broadening from inelastic collisions are suppressed because they shift the outgoing hadron to lower z. Broadening from elastic collisions is present and can be estimated from known cross-sections. An upper bound is taken by setting $l_p=0$ and choosing $A = 208$. For this extreme case, the contribution of elastic pion rescattering to broadening is $0.03\,GeV^2$. While this is not negligible, it is reduced for smaller nuclei and non-zero l_p, as well as potentially being reduced by other effects that increase nuclear transparency.
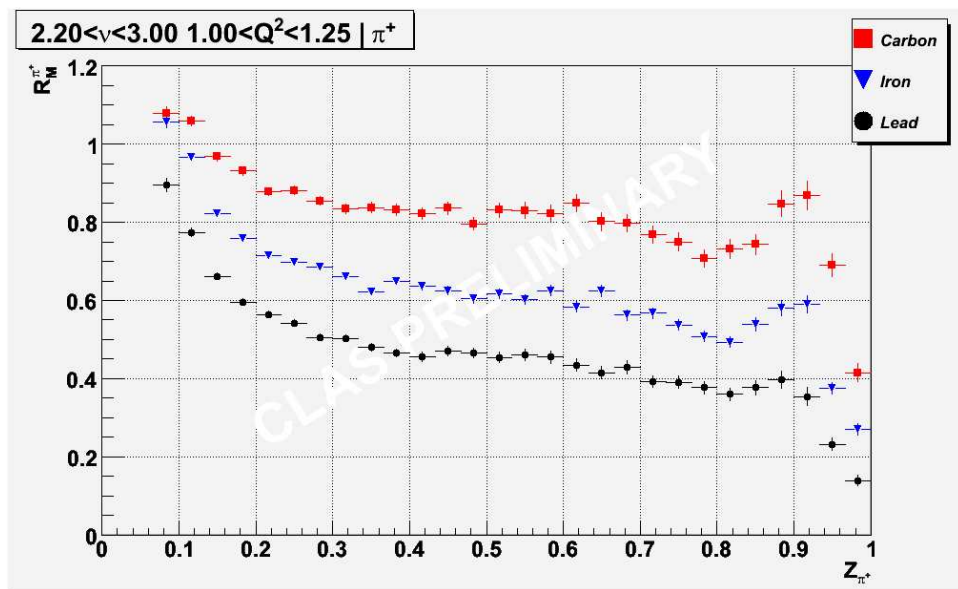

Figure 9: Preliminary data from the CLAS EG2 5.0 GeV data for the hadronic multiplicity ratio $R_M^{\pi^+}$ for positive pions in carbon (bottom), iron, and lead(top).

4.4.2 Extracting the formation time

Formation times are expected to depend on hadron species. Intercomparison of systematic features from a variety of hadrons is expected to yield global insight into what the fundamental dependencies are, e.g. on hadron size, mass, or other hadronic properties.

The derivation of the formation time from data is accomplished through measurements of hadron attenuation. An example of preliminary hadron attenuation results from the 5.0 GeV CLAS EG2 data is given in Fig. 9. It is necessary to use a model to derive quantitative information from the data. In the analysis of the HERMES nitrogen data [7] a procedure

by Biallas and Chmaj [12] was adapted to derive formation lengths for pions. The technique is classical, however, it illustrates the basic ideas. In this procedure, the probability that the propagating object is a quark is $P_q(z) = \exp(-z/\tau)$, and the probability that it is a pre-hadron or hadron is $P_h(z) = 1 - P_q(z)$, where z is the longitudinal coordinate. The probability that the propagating object does not interact with a single nucleon is

$$S_A(b, z) = 1 - \sigma_q \int_z^\infty dz' \rho_A(b, z') P_q(z' - z) - \sigma_h \int_z^\infty dz' \rho_A(b, z') P_h(z' - z) \tag{13}$$

where b is the transverse coordinate, z is the longitudinal coordinate, and σ_q, σ_h are effective interaction cross sections for the quark and the hadron. The hadronic multiplicity ratio is taken as the ratio of the number of hadrons produced from nucleus A to the number from an elementary target, which is then written as:

$$R_M^h = \frac{dn_A}{dn_1} = \int d^2b \int_{-\infty}^\infty dz \; \rho_A(b, z) \; [S_A(b, z)]^{A-1} \tag{14}$$

The HERMES analysis using this technique found good agreement with their data using the formula:

$$\tau = 1.4\nu(1 - z_h)\text{fm/GeV} \tag{15}$$

and found $\sigma_q \approx 0$ and $\sigma_h \approx$ 25 mb as expected from fundamental considerations.

This analysis was a very simple one, and yet it was sufficient to completely rule out several functional forms, including one connected to the Lund model picture. This is an example of where the analysis did not make a distinction between production time and formation time, referring to the cumulative effect of both as 'formation time.' While simple, it demonstrates the principle that such analyses of hadron attenuation data can be carried out reliably. In the case of the proposed data, one natural extension is to characterize the production length using p_T broadening alone, and incorporate those results into subsequent formation length analyses. The framework for more sophisticated procedures to extract formation lengths will be developed over the next few years in conjunction with the international community of theorists engaged in these topics.[7]

4.5   Summary

In this section, a description of the definition and expected sizes of the production time τ_p and the formation time τ_f have been given. The methods to extract these quantities from semi-

---

[7]For a recent workshop on these topics representing a portion of this community, see http://conferences.jlab.org/ECT/program.html

inclusive deep inelastic scattering from nuclei have been outlined. It should be emphasized that the concepts outlined here are not model-dependent constructs. The existence of a finite production length is guaranteed by the confinement property of QCD. The form of equation 4 is given purely by conservation of energy. The existence of a non-zero hadron formation length is guaranteed by causality and relativity. The forms of the expressions for partonic energy loss in vacuum and in-medium are formed from Lorentz invariants. These constraints are fundamental and general. The unknown factors are primarily the coefficients that enter into these expressions, which can be determined by experiment.

5 Previous measurements

One of the pioneering measurements of the hadronization length was done in the 1970's at SLAC [31]. By comparing the attenuation of the number of hadrons produced from nuclei compared with deuterium, normalized to the number of DIS events in each case, they concluded that the hadronization occurred within the distance scale of the nucleus (averaged over the Q^2 and ν kinematics of their DIS events). Although their statistical uncertainties were large, the technique of the multiplicity ratio continues to be valuable today.

Additional data on the multiplicity ratio was measured by the E665 experiment at Fermilab [3] and the EMC experiment [10] using ultra-high-energy muons on various nuclear targets from C to Pb. These data confirmed the fact that hadrons at high z are attenuated in nuclei compared with deuterium. Since particles with $z > 0.5$ are typically considered to be the leading hadron (containing the struck quark), the attenuation in nuclei suggested that hadronization was taking place inside the nucleus. In addition, the response of nuclei to DIS events was measured by detecting low-energy neutrons at backward angles [4] which come from thermalization of the residual nucleus. These data showed clearly that the majority of DIS events in Ca left a "cold" residual nucleus, whereas in a Pb target the residual nucleus was "hot" as expected for hadronization inside the nuclear radius. Although limited in statistics, the E665 results provided motivation for the next generation of experiments at HERMES and CLAS.

The HERMES collaboration published an impressive set of data on the multiplicity ratio for a variety of hadrons ($\pi^\pm$, π^0, $K^\pm$, p, $\bar{p}$) from ^{14}N and Kr targets [6]. These data showed, for the first time, a clear trend of more attenuation as z increases (averaged over Q^2 and $\nu > 7$). They also observed less attenuation as ν increases (averaged over Q^2 and $z > 0.2$). Both of these trends were predicted by theoretical models based on increasing formation time as a function of ν and effective string tensions in the medium. In addition, HERMES found that the multiplicity ratio depends on p_T and that R^h_M is maximal and rising above unity for high p_T.

These data have been the subject of a number of theoretical models in recent years [26] [37] [18] [8] [1], and show definitively that the hadrons are not fully dressed as they propagate through the nucleus, else models that properly describe final state interactions (FSI) for a wide range of hadron-scattering reactions cannot predict the HERMES multiplicity ratios. As a result of having precise data for multiplicity ratios and p_T-broadening, theorists now have the information they need to construct effective models of the process by which a struck quark goes from deconfinement to confinement inside a hadron. Several models now show

that a period of "pre-hadron" propagation is likely, where the object under consideration (usually a $q\bar{q}$ pair or qqq triplet) is not fully dressed, and hence is more transparent to the nuclear medium. This interpretation would not be possible without the experimental data as a basis.

Recently, the EG2 experiment at CLAS has taken data at 5.0 GeV and obtained an unprecidented statistics for hadronization from several nuclei (carbon, iron, and lead). With the EG2 data, it is now possible to measure the multiplicity ratio with significantly smaller uncertainties than for the HERMES data, and to measure these ratios for small bins in Q^2, ν and z. Preliminary results have been obtained for pions [20] and kaons [21]. These data show strong attenuation effects, and follow similar trends as the HERMES data. The precision of the EG2 data will further constrain theoretical models, as described in the previous section. The one disadvantage of the EG2 data is that the range in Q^2 and ν is limited to the edge of the onset of DIS. With the 12 GeV upgrade and the CLAS12 detector, the EG2 data can be extended far into the DIS range where theoretical interpretation of the results is cleaner.

6 Experimental Details and Analysis Procedures

The experiment will be carried out using the CLAS12 detector. A description of the detector design is given in Ref. [17]. The principal features are: (1) the identification of the scattered electron and measurement of its kinematics, (2) the identification of associated hadrons and their kinematics, (3) simulations of the detector acceptances for all particles over a range of kinematic observables. Each of these points will be addressed briefly in the sections below. Because the CLAS12 detector is still in the design stage, it is not possible to present detailed information about the expected detector performance. However, the broader goals of the detector design are understood and will be used to estimate the resolutions and acceptances of the proposed measurements. More details about the spectrometer are available in a separate document [17].

6.1 Electron Identification

In CLAS12, two Cerenkov detectors will be used, one for π^-/e^- separation at low energies (the low threshold CC) and one at high energies (the high threshold CC). The combination of the CC's enable electron identification up to 5 GeV. Above this energy, the forward-angle electromagnetic calorimeter will be used for electron identification, as pions will produce different shower characteristics as compared with electrons. The success of π^-/e^- separation
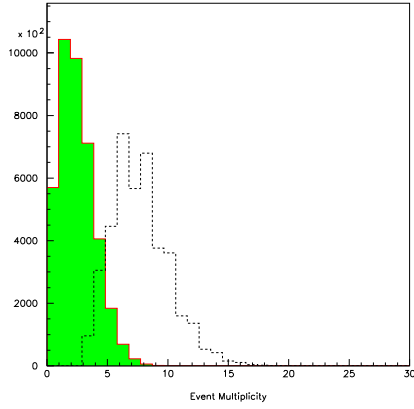
Figure 10: Event multiplicity (i.e., number of hadrons) generated (dotted) and reconstructed (solid) in simulations using the PYTHIA event generator.
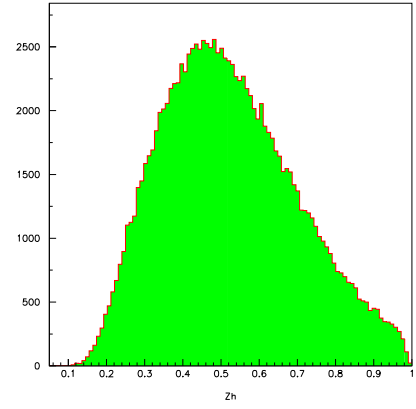

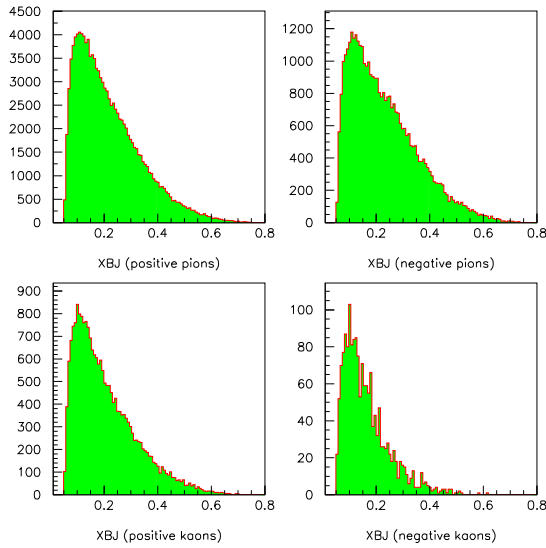Figure 12: The z-distribution of hadrons in the PYTHIA simulations.

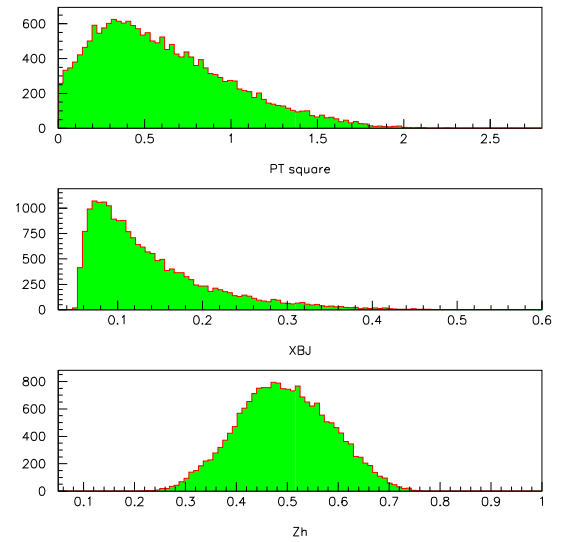Figure 11: The x_{Bj}-distribution for the various particles shown for the PYTHIA simulations.

Figure 13: The distributions in p_T, x_{Bj} and z for a subset of the hadrons in the PYTHIA simulations.

34

up to 6 GeV has already been demonstrated by CLAS, and so the similar techniques employed in CLAS12 are expected to result in clean electron ID. Simulations of the ratio of inner/outer calorimeter deposition by pions and electrons is in progress. The light collection efficiency of the CC's has been studied[17].

6.2 Hadron Identification

A broad range of hadron identification issues are relevant for these measurements. Hadrons that are directly measured place the most stringent constraints since high energy hadrons are the primary focus. Hadrons such as the Λ, ϕ, or K^0 that decay into other hadrons may be simpler to access since their decay products on average are at lower momenta.

An improvement for CLAS12 will be a new time-of-flight (TOF) system with (estimated) 60 ps resolution. In CLAS, the mass of particles can be determined by a combination of momentum (from the drift chambers, DC) and the velocity (from the TOF, currently with about 150 ps resolution). The better resolution is obtained in CLAS12 through use of two layers of somewhat shorter scintillator bars and new phototubes. For example, for a path length of 5.0 m, we can expect K-π separation up to about 3 GeV/c (assuming 4σ timing separation) and p-π separation up to about 6 GeV/c. Beyond these momenta, some particle ID can be obtained by using the low-threshold CC at forward angles. While this situation is not ideal for charged kaon detection, the small contamination of kaons in the pion sample (typically about 1%) should not adversely affect the hadronization studies of charged pions. Charged pions at high energies can be positively identified in the LTCC and HTCC. Another important improvement for CLAS12 is the preshower calorimeter, which will permit measurement of π^0s up to energies beyond 11 GeV.

6.3 Acceptances for various final states

A number of kinematic distributions are shown for the CLAS12 detector in Figs. 10 to 30. Many of these distributions look similar to the current CLAS detector, except the range of the kinematics is expanded for 11 GeV electrons. Of particular interest is the ability of CLAS12 to identify the various types of final state hadrons. Using only TOF and momentum, the typical plot of β (velocity) versus p (momentum) shown in Fig. 22 shows that pions are well separated from kaons up to 3 GeV, and protons are well separated up to about 6 GeV. Clearly, particle identification (PID) is an important part of understanding the hadronization process, and various experimental techniques must be applied to obtain good PID with the CLAS12 detector.
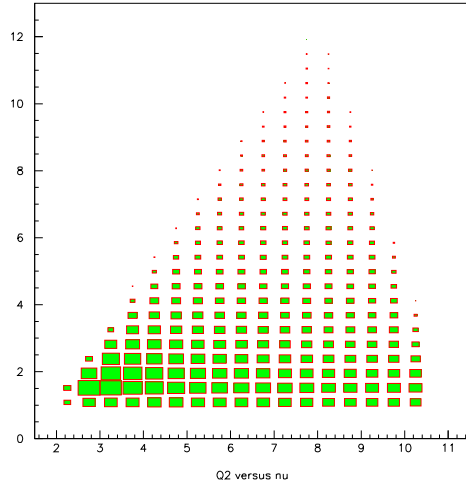
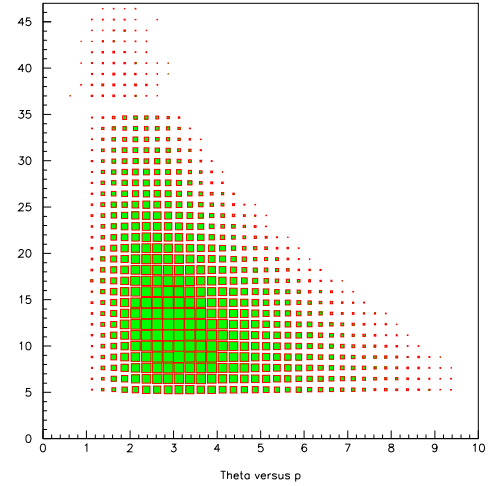Figure 14: Two-dimensional density plot of the distribution of Q^2 versus ν for the PYTHIA simulations.

Figure 16: The distribution of polar angle θ versus the momentum ν for outbending particles in CLAS12 for the PYTHIA simulations.
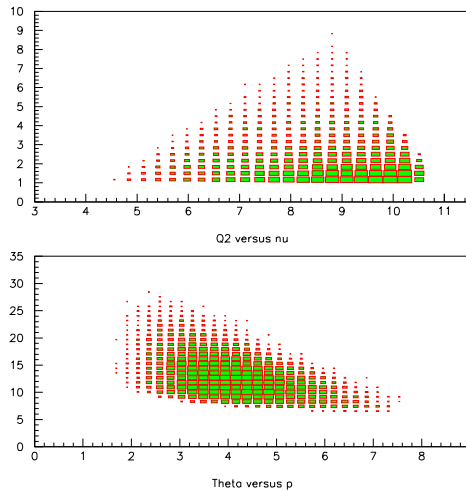

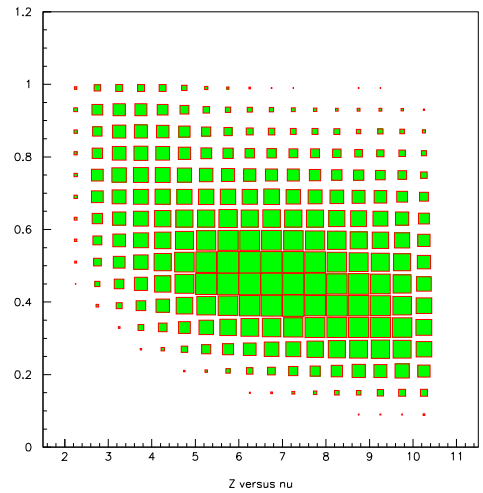Figure 15: Q^2 vs. ν and θ vs. p for antiprotons from the PYTHIA simulations.

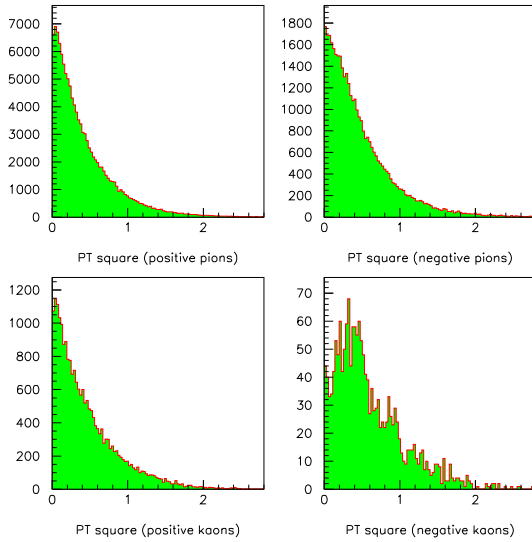Figure 17: The distribution of z vs. ν for positive particles from the PYTHIA simulations.

36

Figure 18: The transverse momentum (from the direction of the virtual photon) for the particles shown in the PYTHIA simulations.
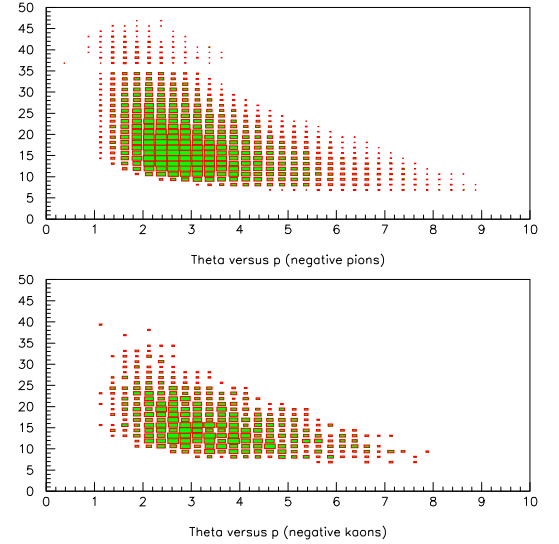
Figure 19: The distributions of Q^2 vs. ν and θ vs. p for inbending particles in CLAS12 from the PYTHIA simulations.

Rather than facing the difficult task of identifying charged kaons cleanly at high momenta, a better approach is to go after neutral kaons through their decay $K_s^0 \to \pi^+\pi^-$. Preliminary simulations have been performed using the PYTHIA event generator and a fast Monte Carlo that includes the resolutions expected for CLAS12. The results are shown in Fig. 31 where the invariant mass of any $\pi^+\pi^-$ pair found in the simulated event is shown. The K^0 shows up as a spike in the mass spectrum for the generated events (left plot) and is still clearly visible after detection in CLAS12 (right plot).

The invariant mass in the $p\pi^-$ system is shown in Fig. 23. Here the Λ peaks is clearly visible and has little background in the region of the peak from fragmentation events. Similarly, the two-photon invariant mass shown in Fig. 38 indicates that the π^o and η will be accessible.

6.4 Resolution issues

The expected CLAS12 resolutions are more than adequate for most of the quantities to be measured, since the typical bin size for these analyses will be, e.g., 1 GeV^2 for Q^2, 1 GeV
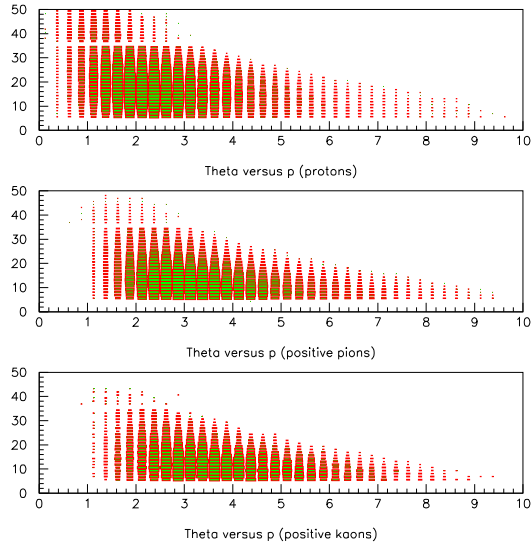
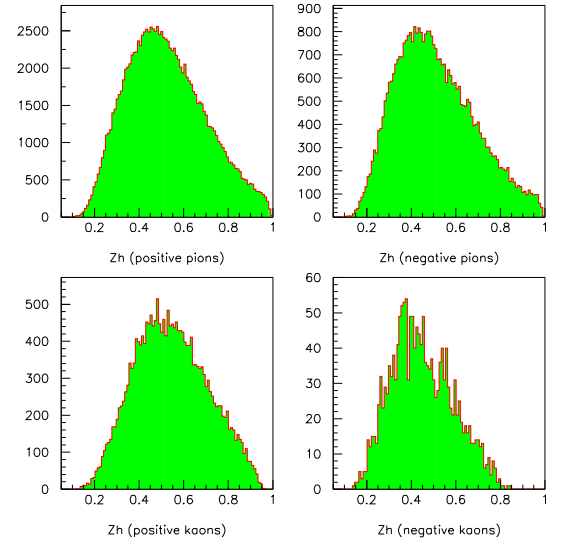Figure 20: The distribution of θ vs. p for positive particles shown from the PYTHIA simulations.

Figure 21: Distribution of z for the particles shown from the PYTHIA simulations.

for ν, etc. The exception concerns the measurement of Δp_T^2, where the expected magnitude is in the range 0.05-0.10 GeV^2. The resolution in p_T^2 is dominated by the CLAS12 angular resolution, while the momentum resolution plays a smaller role. The resolution has been simulated using the standard CLAS12 parametric acceptance and resolution function and the results are shown in Fig. 32 and Fig. 33. A 1 GeV minimum energy is required of the pion in these figures, which is consistent with the minimum energy expected for, e.g., $z = 0.5$ and $\nu = 2\ GeV$, the lowest value of ν accessible ($z\nu = E_h$). As can be seen from the figures, the expected resolution for π^+ is 0.15% and for π^- it is 0.16%, and the distribution is approximately Gaussian. Since the p_T^2 spectra are dominated by values of p_T that are less than 0.5 GeV^2, the typical resolution is less than $0.01 GeV^2$, and therefore the resolution is well-suited to measure the broadening at the $0.05 - 0.10\ GeV^2$ level.

7   Rate Estimates and Expected Results

Rate estimates have been performed by calculation with the standard monte carlo codes LEPTO [22] and PYTHIA [34], as well as phase space generators. Table 1 shows example
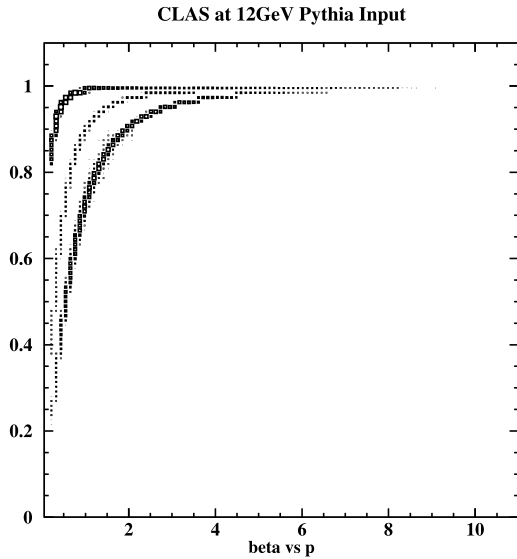
Figure 22: Distribution of β vs. p in the PYTHIA simulations, showing the clean TOF separation of kaons and pions below about 3 GeV and for protons below about 6 GeV.
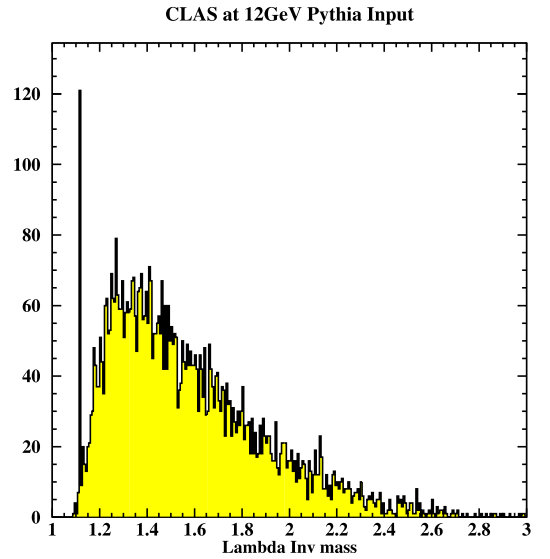
Figure 23: The invariant mass of the $p\pi^-$ pairs in the PYTHIA simulations, showing a sharp peak for the Λ at 1.115 GeV and a broad background at higher masses.

raw production rates from LEPTO for hadrons with $c\tau$ larger than the radius of the lead nucleus. This condition is desirable to avoid ambiguities due to particles potentially decaying within the nucleus. Other columns in Table 1 show the hadron mass, flavor content, and detection channel in CLAS12, in addition to the lifetimes and the rates. It is clear that high-statistics data for this spectrum of hadrons will permit systematic studies of, e.g., the mass dependence and flavor dependence of hadronic formation times.

Following event generation, for selected particles studies were performed using the standard CLAS12 parametric acceptance and resolution function. All plots of simulated data in this proposal have been made using this parametric function.

A plot that concisely demonstrates the single-particle acceptance is shown in Fig. 34. The simulated data were generated using Pythia with 11 GeV beam, the hollow histogram bars show the thrown data, and the shaded bars superimposed show the data that passed
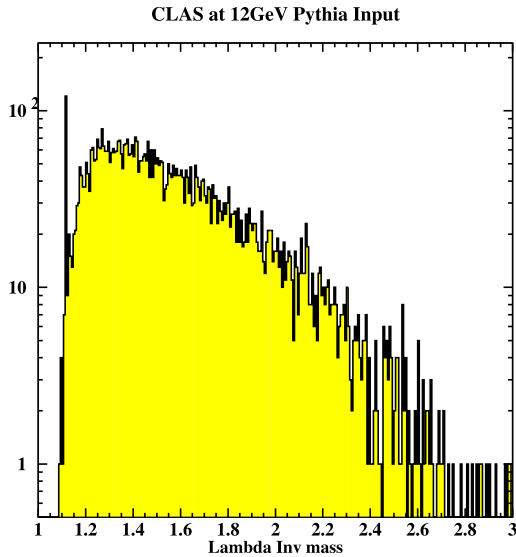
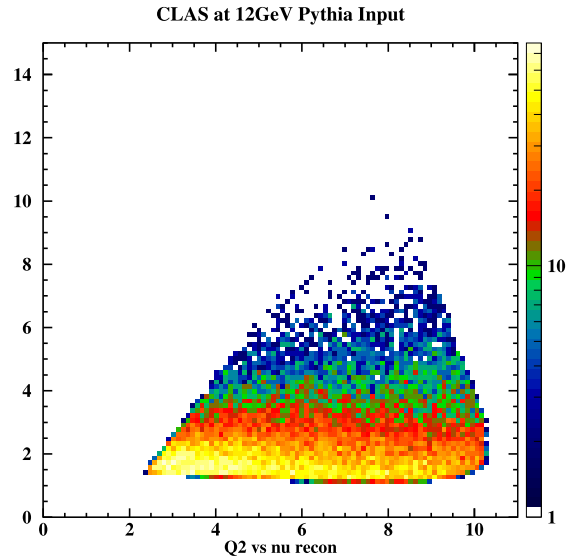Figure 24: Same as previous figure, except on a log scale.

Figure 25: The Q^2 vs. ν distribution for reconstructed events in CLAS12 from the PYTHIA simulations.

the acceptance tests. The basic pattern is a familiar one from the experience with CLAS. High-energy, forward charged particles such as the ones of interest in this proposal have a single-particle acceptance of approximately 50%. Positively charged particles have somewhat higher acceptance (the torus field is chosen so that positive particles bend outward, away from the beam axis). Thus, the acceptances for π^+, K^+, and protons are similar to each other, as are the acceptances for π^-, K^-, and antiprotons. For fragmentation events in which one hadron is detected, the electron and the hadron are largely uncorrelated in direction and thus the overall event acceptance is approximately the product of the electron acceptance and the hadron acceptance. This ends up being in the range of 20-25%.

Ideally, there would be a well-defined, proven procedure for extracting the quark production time and the hadron formation times. At the present time, the ideas for how to carry out such a procedure are at an early stage and cannot be fully validated without a full 11 GeV data set. Therefore, the beam time request is driven by several factors that are known to some level of accuracy and are important for developing such a high-level analysis
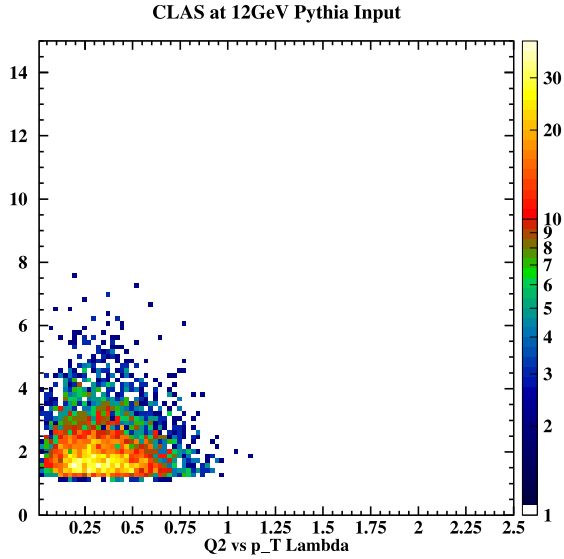
40

Figure 26: The distribution of Q^2 vs. p_T for Λ particles in the PYTHIA simulations.
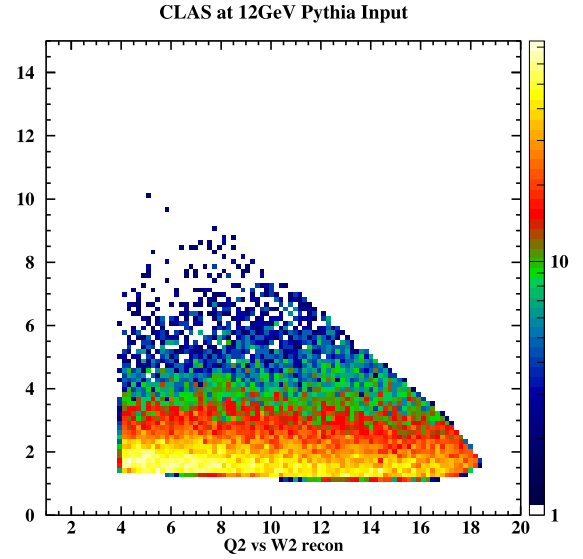
Figure 27: The distribution of Q^2 vs. W^2 reconstructed in CLAS12 in the PYTHIA simulations.

procedure:

1. In order to map out the length dependence of the production length and formation length in multi-variable bins, the data need to span five or six nuclei

2. For each nucleus, there are four variables known to affect the hadron attenuation: Q^2, ν, p_T^2, and z. Once cuts are made on each of these, the statistical accuracy must be no greater than the systematic errors, which are at the level of approximately 4%.

3. There are several low-rate processes of high physics interest that drive the request:

   - antiproton rate
   - phi rate

It is very desirable to measure the Q^2 dependence for these low-rate reactions in order to pin down the reaction mechanisms involved.

41

To illustrate point number 1, in Fig 8 is shown data for p_T broadening vs. $A^{1/3}$ from the CLAS EG2 experiment at 5 GeV for carbon, iron, and lead. The data suggest a possible plateauing, which is what one would expect if the production time τ_p for this bin in Q^2, ν, and z is shorter than the radius of the lead target. However, with only three data points, it is not possible to characterize the shape of this curve adequately. Since the variation in nuclear size is the standard by which distance scales are measured in this experiment, it is very important to have enough nuclei to determine, for example, the point at which the plateau begins to form in order to compare with theoretical predictions.

To illustrate points number 2 and 3, consider the rates achievable for anti-protons in two Q^2 bins, from 1–2 GeV^2 and > 2 GeV^2, for large ν. The rates for anti-protons are estimated using the PYTHIA generator and FASTMC for CLAS12 detector simulation. A luminosity of 10^{35} cm^{-2} s^{-1} is assumed. Integrating over all variables, the anti-proton rates from the proton target is 0.48/s and from the neutron target is 0.3/s. Tables 2 and 3 indicate the rates in bins in z.
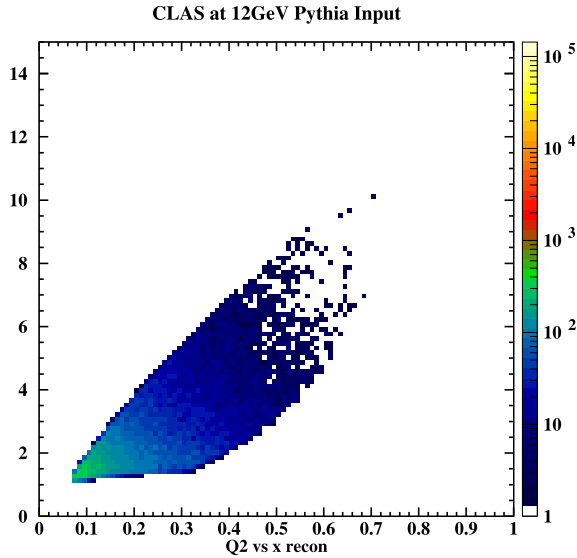

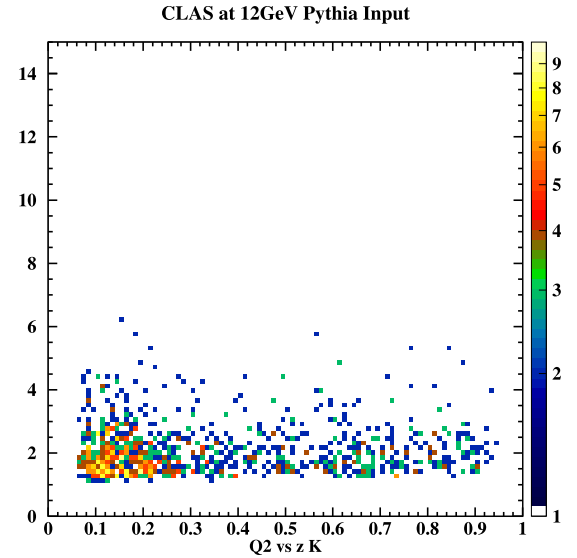Figure 28: The distribution of Q^2 vs. x reconstructed in CLAS12 in the PYTHIA simulations.

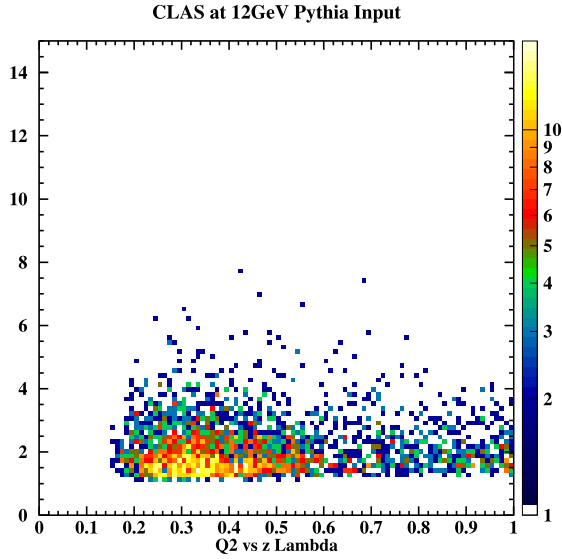Figure 29: Same as one of the previous figures, except for kaons.

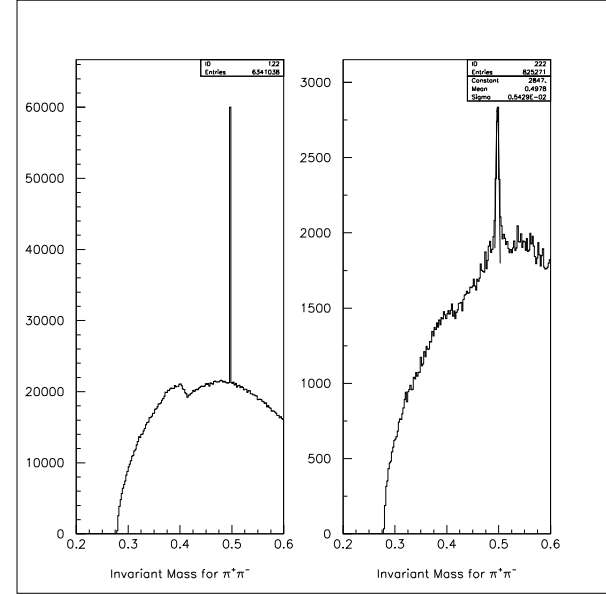Figure 30: Same as the previous figure, except for Λ's.

Figure 31: Generated and reconstructed invariant mass spectrum for $\pi^+\pi^-$ pairs from the PYTHIA simulations.

In order to achieve 3% statistics for antiprotons in a bin in ν, z, Q^2 and at $p_T > 1 \ GeV^2$ for six nuclear targets (plus deuterium) approximately 100 days of beam time would be required. A similar accuracy for ϕ mesons would require several times as much beam time. As a compromise, an exploratory measurement for these particles could be accomplished in approximately 60 days. This would probe the Q^2 dependence for the antiproton up to approximately 6 GeV^2 with good accuracy. Similarly, an exploratory measurement of the ϕ could be carried out that would probe up to approximately 2 GeV^2. Thus, the beam time request for these measurements is 60 PAC days. A more refined calculation can be performed for the future PACs at which beam time allocations will be made.

An idea of the expected results is given in Figures 35, 36, and 37 for the hadronic multiplicity ratio vs. z for positive pions and four different target nuclei. There is an enormous kinematic coverage for π^+ with the 11 GeV beam conditions. The coverage is naturally more limited for the lower-rate final states.
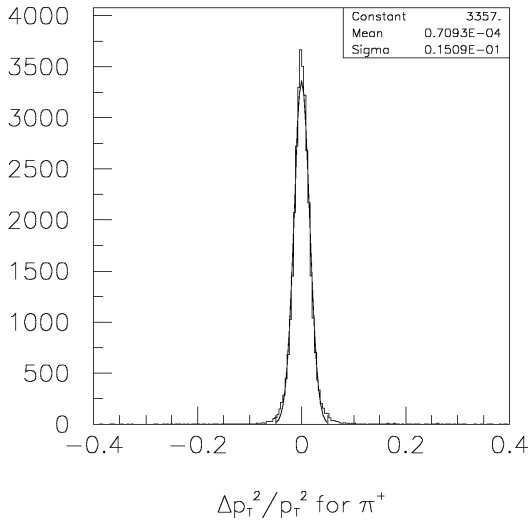
Figure 32: Resolution in Δp_T^2 for positive pions with energies greater than 1 GeV.
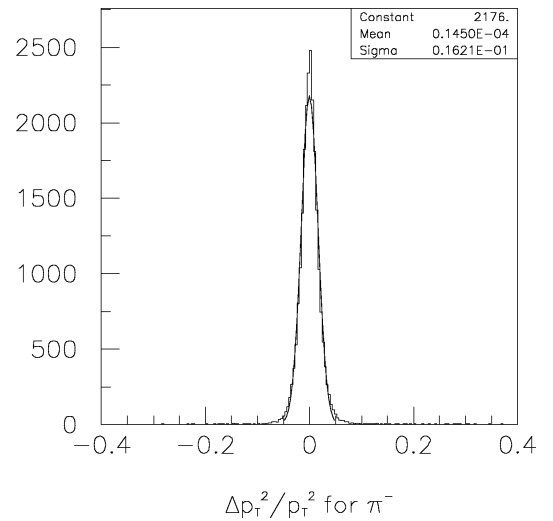
Figure 33: Resolution in Δp_T^2 for negative pions with energies greater than 1 GeV.

8 Connections to Other Subfields of Nuclear and Particle Physics

The primary topics of this proposal are to determine the quark production time and hadron formation times for a variety of hadrons. The interest in these quantities comes from their close connection to quark confinement in forming systems. In addition to this motivation, there are strong connections to other subfields that provide further motivation to study these topics. The study of quark energy loss is critically important to the observation of the highly correlated state of hot dense matter at the Relativisitic Heavy Ion Collider (RHIC) and the extension of those studies within the next few years at the Large Hadron Collider (LHC). Experimental estimates of the quark energy loss have primarily come from the Fermilab experiments using the Drell-Yan reaction in proton-nucleus collisions. Finally, hadron formation lengths have important implications for the experimental study of neutrino oscillations.

8.1 RHIC and LHC

The driving motivation for building RHIC was to discover and study a 'quark-gluon plasma,' a hot and dense medium formed in high-energy collisions of heavy nuclei. These ideas were

Table 1: Final-state hadrons potentially accessible for formation length and transverse momentum broadening studies in CLAS12. The rate estimates were obtained from the LEPTO event generator for an 11 GeV incident electron beam. (The criteria for selection of these particles was that $c\tau$ should be larger than nuclear dimensions, and their decay channels should be measurable by CLAS12.)

hadron	$c\tau$	mass (GeV)	flavor content	detection channel	Production rate per 1k DIS events
π^0	25 nm	0.13	$u\bar{u}d\bar{d}$	$\gamma\gamma$	1100
π^+	7.8 m	0.14	$u\bar{d}$	direct	1000
π^-	7.8 m	0.14	$d\bar{u}$	direct	1000
η	0.17 nm	0.55	$u\bar{u}d\bar{d}s\bar{s}$	$\gamma\gamma$	120
ω	23 fm	0.78	$u\bar{u}d\bar{d}s\bar{s}$	$\pi^+\pi^-\pi^0$	170
η'	0.98 pm	0.96	$u\bar{u}d\bar{d}s\bar{s}$	$\pi^+\pi^-\eta$	27
ϕ	44 fm	1.0	$u\bar{u}d\bar{d}s\bar{s}$	K^+K^-	0.8
$f1$	8 fm	1.3	$u\bar{u}d\bar{d}s\bar{s}$	$\pi\pi\pi\pi$	-
K^+	3.7 m	0.49	$u\bar{s}$	direct	75
K^-	3.7 m	0.49	$\bar{u}s$	direct	25
K^0	27 mm	0.50	$d\bar{s}$	$\pi^+\pi^-$	42
p	stable	0.94	ud	direct	530
$\bar{p}$	stable	0.94	$\bar{u}\bar{d}$	direct	3
Λ	79 mm	1.1	uds	$p\pi^-$	72
$\Lambda(1520)$	13 fm	1.5	uds	$p\pi^-$	-
Σ^+	24 mm	1.2	us	$p\pi^0$	6
Σ^0	22 pm	1.2	uds	$\Lambda\gamma$	11
Ξ^0	87 mm	1.3	us	$\Lambda\pi^0$	0.6
Ξ^-	49 mm	1.3	ds	$\Lambda\pi^-$	0.9

developed nearly three decades ago [33]. Experimentally, what has been found behaves like an ideal classical liquid, where the constituents interact strongly and there is minimal viscosity. The primary evidence that a hot, dense state of matter has been formed is the observation of **jet quenching**.

Jet quenching is the observation of a suppression of leading hadrons emerging from a

z bins	Rates off proton target $(\times 10^{-5}s^{-1})$	Rates off neutron target $(\times 10^{-5}s^{-1})$
$0.2 \leq z < 0.3$	346	195
$0.3 \leq z < 0.4$	2227	1558
$0.4 \leq z < 0.5$	3559	2949
$0.5 \leq z < 0.6$	3181	2787
$0.6 \leq z < 0.7$	1506	1362
$0.7 \leq z < 0.8$	123	49

Table 2: The estimated rates for anti-proton production within CLAS12 acceptance using the PYTHIA generator and assuming the luminosity to be $10^{35}cm^{-2}s^{-1}$. The considered bin is $\nu > 9$ GeV and $Q^2 \leq 2$ GeV^2

z bins	Rates off proton target $(\times 10^{-5}s^{-1})$	Rates off neutron target $(\times 10^{-5}s^{-1})$
$0.2 \leq z < 0.3$	162	99
$0.3 \leq z < 0.4$	1503	1032
$0.4 \leq z < 0.5$	3060	1742
$0.5 \leq z < 0.6$	2241	1656
$0.6 \leq z < 0.7$	1003	666
$0.7 \leq z < 0.8$	112	26

Table 3: The estimated rates for anti-proton production within CLAS12 acceptance using the PYTHIA generator and assuming the luminosity to be $10^{35}cm^{-2}s^{-1}$. The considered bin is $\nu > 9$ GeV and $Q^2 > 2$ GeV^2
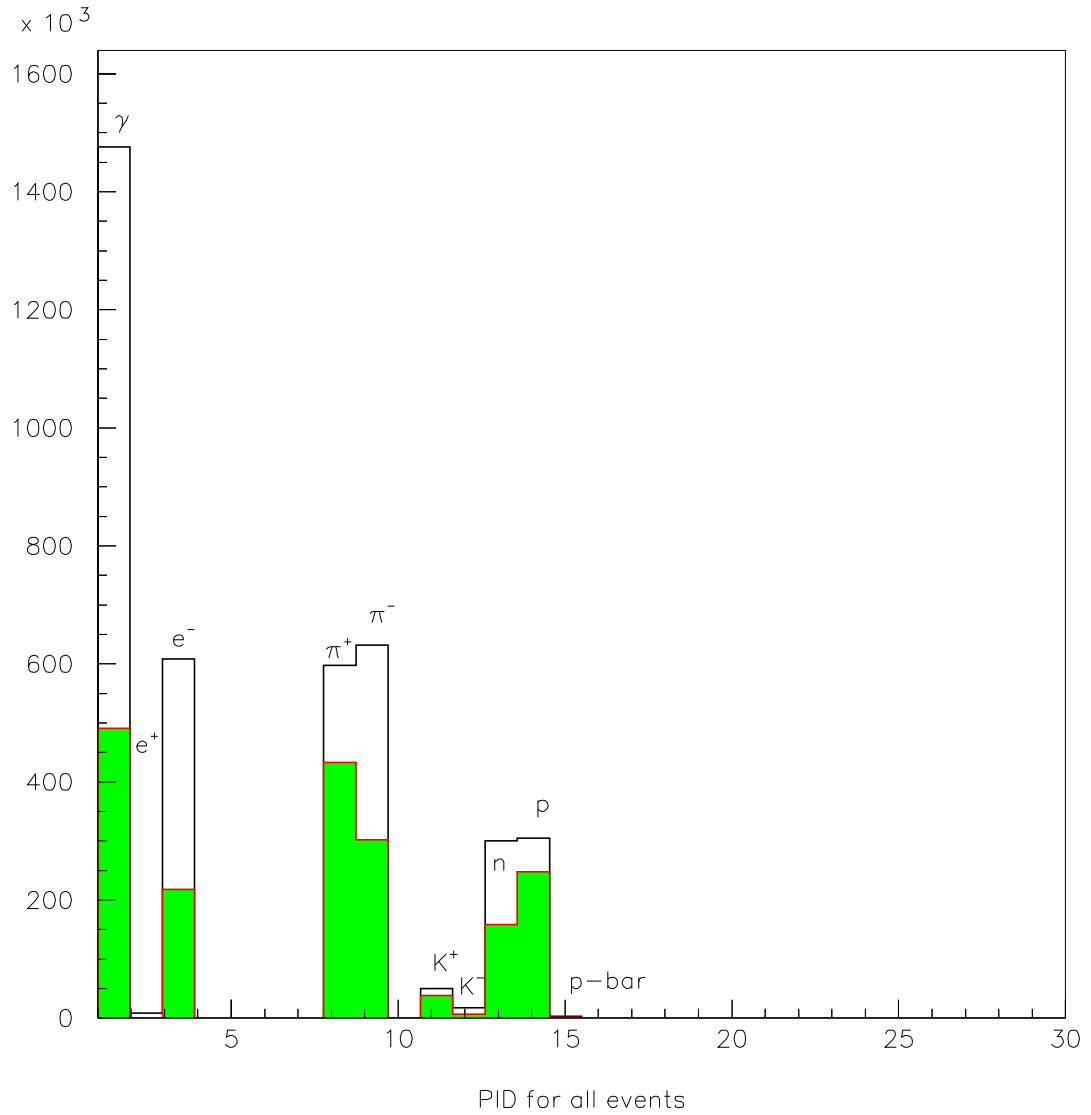
Figure 34: Thrown and reconstructed particles using the standard CLAS12 parametric acceptance function. Open bars indicate thrown particles, solid bars are accepted particles.

heavy ion collision. The suppression is relative to the pattern of leading hadrons emerging from, e.g., deuterium-nucleus collisions, where the medium is 'cold' and of normal nuclear density. It is a dramatically large suppression, as much as a factor of five for central collisions, as can be seen in Fig. 8.1.
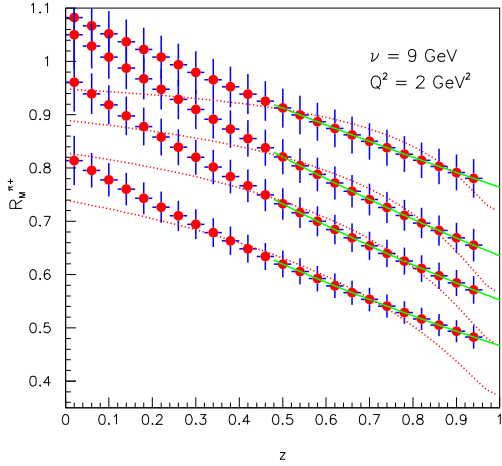
Figure 35: Z dependence of the hadronic multiplicity ratio for (top to bottom) ^{14}N, ^{40}Ar, ^{84}Kr, ^{197}Au for $\nu = 9\ GeV$ and $Q^2 = 2\ GeV^2$. The solid line is a gluon bremsstrahlung model calculation for $z > 0.5$ for pions. The dotted line shows the parameterization based on the HERMES 27 GeV data[7], which is independent of Q^2.
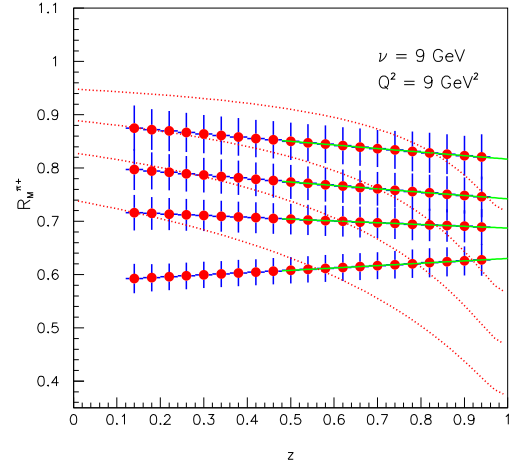
Figure 36: The same plot as in Fig. 35 for $\nu = 9\ GeV$ and $Q^2 = 9\ GeV^2$. The errors shown in both figures are a combination of statistical and systematic errors for 30 days of running at design luminosity. Note the dramatic change in the gluon bremsstrahlung model prediction for the higher Q^2 data.

A related phenomenon is termed 'mono-jet production.' Ordinarily, high energy jets occur in pairs which are directed in opposite directions in the center-of-momentum system, an obvious consequence of a hard quark-quark elementary interation. However, there is clear evidence that one of these two jets is completely extinguished in central collisions when the process is embedded in a heavy-ion reaction[37].

Both jet quenching and mono-jet production are explained by medium-stimulated quark energy loss through gluon radiation, exactly the same phenomenon studied in this proposal. The difference between the RHIC and JLab scenarios is only the temperature and density of the medium. Since the quark energy loss is proportional to the gluon density of the medium, it is much larger in magnitude in the hot dense matter. The importance of the JLab data is that it provides by far the best *experimental* access to the study of this phenomenon available to date. The RHIC analyses of jet quenching rely heavily on theoretical parameterizations of the process, with no experimental cross-check aside from the RHIC data itself. While the dominant explanation of jet quenching is radiative energy loss by gluon emission [36],
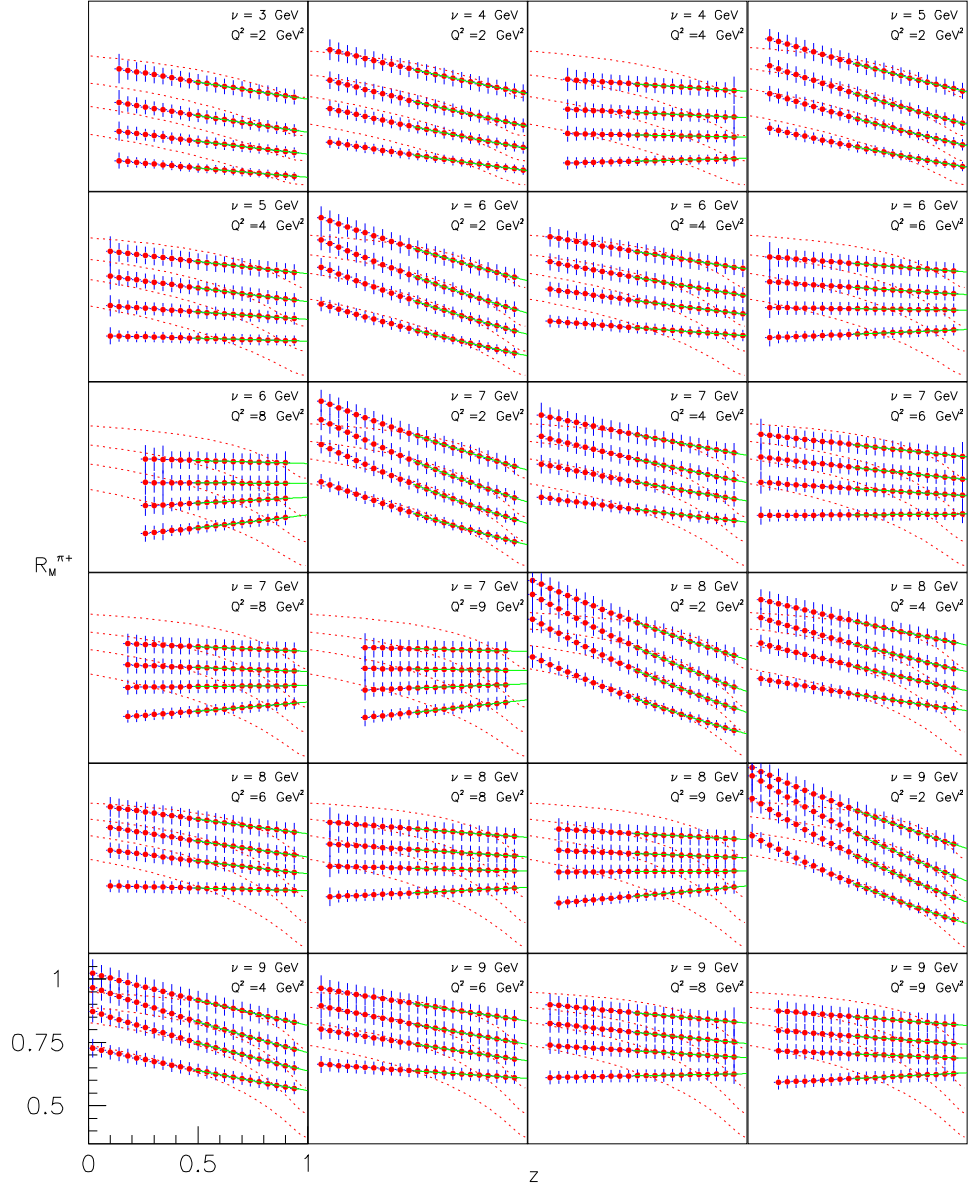
Figure 37: Z dependence of the hadronic multiplicity ratio for (top to bottom in each plot) ^{14}N, ^{40}Ar, ^{84}Kr, ^{197}Au for 24 bins in ν, Q^2. The solid line is a gluon bremsstrahlung model[26] calculation for $z > 0.5$ for pions. The dotted line shows the parameterization based on the HERMES 27 GeV data[7], which is independent of Q^2. 13 bins with $Q^2 = 3$ and $Q^2 = 5 \; GeV^2$ have been omitted to permit readability of this figure.
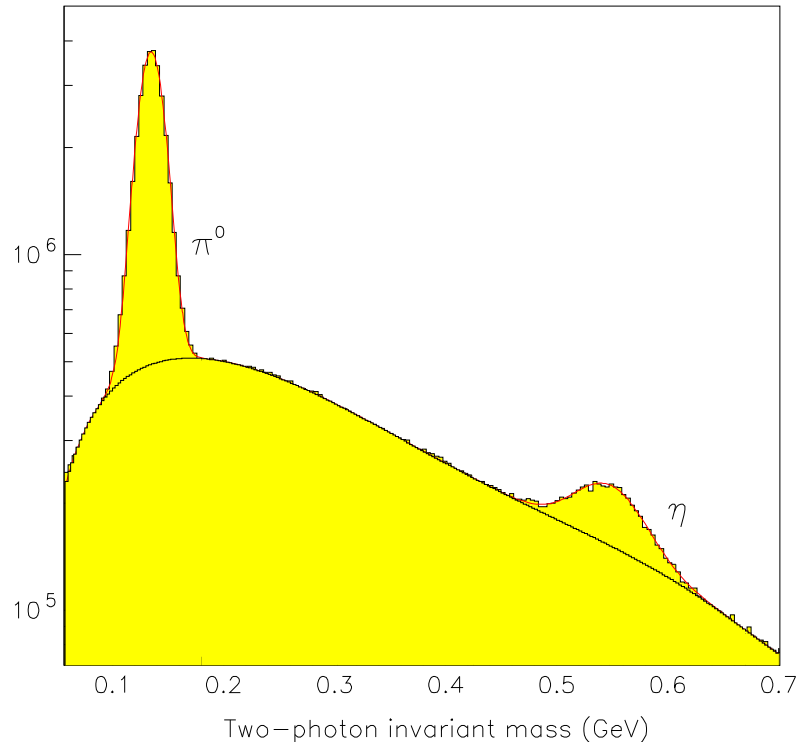
Figure 38: Expected data from a LEPTO simulation at 11 GeV, showing production of neutral pions and eta mesons for a few PAC hours of data acquisition time. A parametric acceptance and resolution function has been applied.

this explanation is not uncontested [26] and it is critical to gain much more experimental evidence against which the RHIC data can be calibrated. When the LHC heavy ion program begins later this decade, the same issues will still be present, making it even more critical to understand the fundamental phenomena at work. It is critical to reliably measure a baseline of quark energy loss in nuclear systems at low temperatures in order to assure its correct application at high temperatures and high densities.

8.2 Drell-Yan

The Drell-Yan (DY) reaction, in which a projectile quark annihilates with a target sea anti-quark, ultimately producing a dilepton pair, has been employed to study nucleon structure as well as nuclear effects for many years [29]. This reaction has been used to estimate the size of quark energy loss and transverse momentum broadening (for a recent analysis, see [24] and references therein). Experiments E772 and E866 at Fermilab consisted of 800 GeV
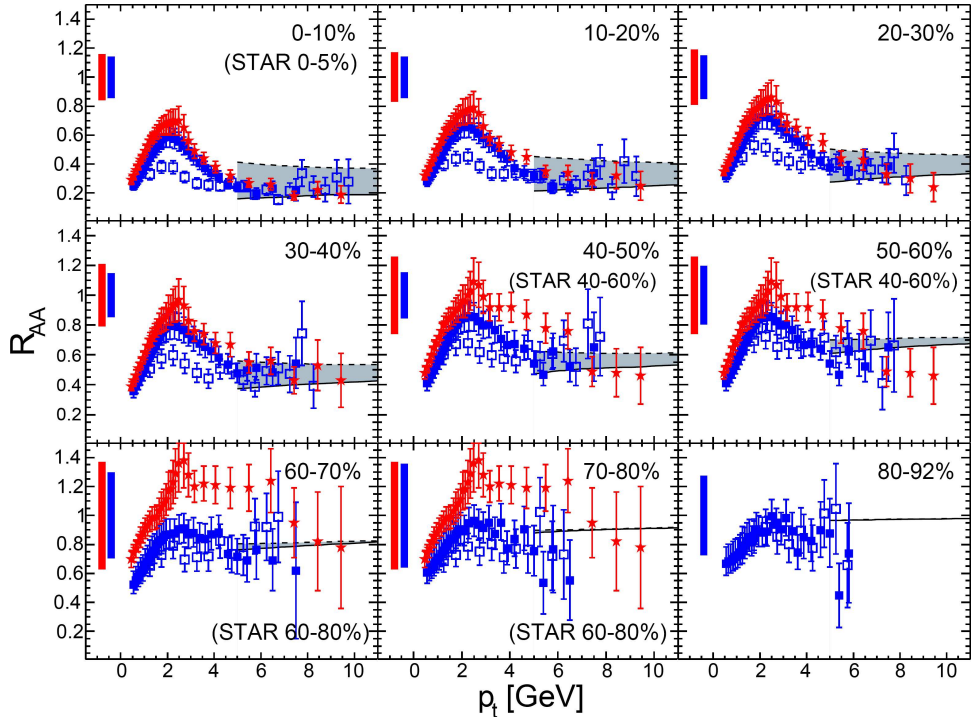
50

Figure 39: $R_{AA}(p_t)$ for different centralities. Data are PHENIX charged hadrons (closed squares) and π^0 (open squares) [5] and STAR charged hadrons (stars) [2].

protons impinging on nuclear targets, measuring dimuons. In principle these data can be used to estimate a value for quark energy loss, however, ambiguities in the theoretical analysis created difficulties in performing a precise extraction; future DY experiments at lower energies will remove the ambiguity, which is associated with separating quark energy loss from the effects of nuclear shadowing. It is strongly desirable to have at least two independent experimental methods to measure the quark energy loss in order to have full confidence in the methods of extraction and the final results. The only two candidates world-wide are the JLab measurements as proposed here, and the low-energy DY measurement proposed at Fermilab.

8.3   Neutrino Oscillations

While the topic of neutrino oscillations would naively appear to be unrelated to the topics in this proposal, there actually is a crucial connection via a practical problem. The accelerator-based neutrino experiments planned in next decade or two will produce neutrino fluxes of

unprecedented magnitude. Such fluxes enable high-precision studies of neutrino oscillations that have previously always been unfeasable due to rate limitations. However, because the experiments still use nuclear targets to take the fullest advantage of the large fluxes, it is now required to understand the systematic nuclear effects that arise. One such effect is the attenuation of hadrons, which can potentially have a very significant influence on the response of the detector systems used for neutrino experiments, e.g., water Cerenkov counters. Without a full characterization of hadron attenuation, it will not be possible to carry out the high-precision studies proposed.

9 Summary and Conclusions

The measurements proposed herein offer an opportunity to obtain completely new information on QCD confinement in forming systems. The measurement of the production time will provide a first experimental look at how far a deconfined quark can propagate before it is confined into a color-singlet hadron. Measurements of the hadron formation lengths for a wide variety of hadrons will for the first time systematically provide insight into the fundamental principles governing how hadrons form. These questions are of high scientific interest, and they are also of high relevance and importance to other subfields of nuclear and particle physics. A comprehensive program of this nature can be carried out with the CLAS12 spectrometer and 11 GeV electron beam in 60 PAC days.

References

[1] A. Accardi, D. Grunewald, V. Muccifora, and H. J. Pirner. Atomic mass dependence of hadron production in deep inelastic scattering on nuclei. *Nucl. Phys.*, A761:67, 2005.

[2] J. Adams et al. *Phys. Rev. Lett.*, 91:172302, 2003. (STAR Coll.).

[3] M. R. Adams et al. *Phys. Rev.*, D50:1836, 1994.

[4] M. R. Adams et al. *Phys. Rev. Lett.*, 74:5198, 1995.

[5] S. S. Adler et al. *Phys. Rev.*, C69:034910, 2004. (PHENIX Coll.).

[6] A. Airapetian et al. *Phys. Lett.*, B577:37, 2003. (HERMES Coll.).

[7] A. Airapetian et al. *Eur. Phys. J.*, C20:2001, 479. (HERMES Coll.).

[8] F. Arleo. Quenching of hadron spectra in dis on nuclear targets. *Eur. Phys. J.*, C30:213, 2003.

[9] X. Artru and G. Mennessier. *Nucl. Phys.*, B70:93, 1974.

[10] J. Ashman et al. *Z. Phys.*, C52:1, 1991. (EMC Coll.).

[11] R. Baier, D. Schiff, and B. F. Zakharov. Energy loss in perturbative qcd. *Ann. Rev. Nucl. Part. Sci.*, 50:37, 2000.

[12] A. Bialas and T. Chmaj. Leptoproduction of hadrons from nuclear targets and fragmentation of quarks into hadrons. *Physics Letters*, 133B:241, 1983.

[13] A. Casher, H. Neuberger, and S. Nussinov. *Phys. Rev.*, D20:179, 1978.

[14] G. Corcella, I. G. Knowles, G. Marchesini, S. Moretti, K. Odagiri, P. Richardson, M. H. Seymour, and B. R. Webber. *JHEP*, 0101:010, 2001.

[15] Y. L. Dokshitzer, V. A. Khoze, A. H. Mueller, and S. I. Troyan. *Basics of Perturbative QCD*. Editions Frontieres, 1991.

[16] V. Del Duca, S. J. Brodsky, and P. Hoyer. *Phys. Rev.*, D46:931, 1992.

[17] L. Elouadrhiri. *An Overview of the CLAS12 Spectrometer.* 2006.

[18] T. Falter, W. Cassing, K. Gallmeister, and U. Mosel. Hadron attenuation in deep inelastic lepton-nucleus scattering. *Phys. Rev.*, C70:054609, 2004.

[19] J. F. Gunion and G. Bertsch. *Phys. Rev.*, D 25:746, 1982.

[20] H. Hakobyan. *EG2 Logbook, unpublished.*

[21] K. Hicks. *EG2 Logbook, unpublished.*

[22] G. Ingelman, A. Edin, and J. Rathsman. Lepto 6.5 - a monte carlo generator for deep inelastic lepton-nucleon scattering. *Computer Physics Communications*, 101:108, 1997.

[23] R. L. Jaffe, F. E. Close, R. G. Roberts, and G. G. Ross. *Physics Letters*, 134B:449, 1984.

[24] M. B. Johnson, B.Z. Kopeliovich, M.J. Leitch, P.L. McGaughey, J. L. Moss, I. K. Potashnikava, and I. Schmidt. *hep-th/0606126*, 2006.

[25] B. Z. Kopeliovich. Private communication.

[26] B. Z. Kopeliovich, J. Nemchik, E. Predazzi, and A. Hayashigaki. *Nucl. Phys.*, A740:211, 2004.

[27] B. Z. Kopeliovich and F. Niedermayer. *Sov. J. Nucl. Phys.*, 42:504, 1985.

[28] B. Z. Kopeliovich and F. Niedermayer. *Yad. Fiz.*, 42:797, 1985.

[29] P. L. McGaughey, J. C. Peng, and J. M. Moss. *Ann. Rev. Nucl. Part. Sci.*, 49:217, 1999.

[30] F. Niedermayer. *Phys. Rev.*, D 25:3494, 1986.

[31] L. S. Osborne et al. *Phys. Rev. Lett.*, 40:1624, 1978.

[32] J. Schwinger. *Phys. Rev.*, 82:1951, 664.

[33] E. V. Shuryak. *Phys. Lett.*, B78:150, 1978.

[34] T. Sjostrand, S. Mrenna, and P. Skands. Pythia 6.4 manual. *JHEP05*, page 026, 2006.

[35] E. Wang and X.-N.Wang. Jet tomography of hot and cold nuclear matter. *Phys. Rev. Lett.*, 89:162301, 2002.

[36] X.-N. Wang. *Phys. Lett.*, B579:299, 2004.

[37] X.-N. Wang. *Nucl. Phys.*, A750:98, 2005.